Tectonophysics 680 (2016) 174–191

Contents lists available at ScienceDirect

Tectonophysics

journal homepage: www.elsevier.com/locate/tecto

Microstructures, deformation mechanisms and seismic properties of a Palaeoproterozoic shear zone: The Mertz shear zone, East-Antarctica

Gaëlle Lamarque [a,*], Jérôme Bascou [a], Claire Maurice [b], Jean-Yves Cottin [a], Nicolas Riel [c], René-Pierre Ménot [a]

[a] Université de Lyon, Université Jean Monnet, UMR CNRS IRD 6524, Laboratoire Magmas et Volcans, 42023 Saint Etienne, France
[b] Microstructures and Processing Department, Ecole nationale supérieure des mines de Saint-Etienne, 158 cours Fauriel, 42023 Saint-Etienne, France
[c] Department of Earth Sciences, Durham University, Science Labs, Durham DH1 3LE, England, United Kingdom

ARTICLE INFO

Article history:
Received 25 July 2015
Received in revised form 25 April 2016
Accepted 9 May 2016
Available online 16 May 2016

Keywords:
Crustal deformation
Shear zone
Microstructures
Crystallographic preferred orientation (CPO)
East Antarctica
Strain localization

ABSTRACT

The Mertz shear zone (MSZ) is a lithospheric scale structure that recorded mid-crustal deformation during the 1.7 Ga orogeny. We performed a microstructural and crystallographic preferred orientation (CPO) study of samples from both mylonites and tectonic boudins that constitute relics of the Terre Adélie Craton (TAC). The deformation is highly accommodated in the MSZ by anastomosed shear bands, which become more scattered elsewhere in the TAC. Most of the MSZ amphibolite-facies mylonites display similar CPO, thermal conditions, intensity of deformation and dominant shear strain. Preserved granulite-facies boudins show both coaxial and non-coaxial strains related to the previous 2.45 Ga event. This former deformation is more penetrative and less localized and shows a deformation gradient, later affected by a major phase of recrystallization during retrogression at 2.42 Ga. Both MSZ samples and granulite-facies tectonic boudins present microstructures that reflect a variety of deformation mechanisms associated with the rock creep that induce contrasted CPO of minerals (quartz, feldspar, biotite, amphibole and orthopyroxene). In particular, we highlight the development of an "uncommon" CPO in orthopyroxene from weakly deformed samples characterized by (010)-planes oriented parallel to the foliation plane, [001]-axes parallel to the stretching lineation and clustering of [100]-axes near the Y structural direction.

Lastly, we computed the seismic properties of the amphibolite and granulite facies rocks in the MSZ area in order to evaluate the contribution of the deformed intermediate and lower continental crust to the seismic anisotropy recorded above the MSZ. Our results reveal that (i) the low content of amphibole and biotite in the rock formations of the TAC, and (ii) the interactions between the CPO of the different mineralogical phases, generate a seismically isotropic crust. Thus, the seismic anisotropy recorded by the seismic stations of the TAC, including the MSZ, must be due to mantle rather than crustal structures.

1. Introduction

Lithospheric scale shear zones are described as localization areas where the deformation is localized between adjacent terrains and dominated principally by simple shear. In association with faults in the upper crust, they profoundly influence the formation and the evolution of mountain belts and sedimentary basins (Alsop and Holdsworth, 2004). They are thus key regions that provide us insights into deformation, rheology and dynamics of the lithosphere (Burov, 2011; Vauchez et al., 2012).

Depending on the interplay of different physical parameters such as far-field forces, lithology, pressure and temperature conditions, fluid transfer and strain rate, various deformation mechanisms can be activated. This has a strong influence on the resulting microstructures, such as grain shape and size, and crystallographic preferred orientation associated with dominant slip systems in minerals undergoing dislocation creep deformation (Nicolas and Poirier, 1976; Passchier and Trouw, 1996; Vauchez et al., 2012).

The Mertz shear zone (MSZ) in Antarctica is a lithospheric shear zone that separates the 2.4 Ga old granulite and amphibolite facies terrains to the west from a 0.5 Ga old intrusive complex related to the Ross Orogeny to the east. Available geochronological data (40Ar/39Ar on amphibole and biotite) show that the MSZ was active at 1.7 and 1.5 Ga in amphibolite and greenschist facies conditions, respectively (Di Vincenzo et al., 2007; Duclaux et al., 2008). Older granulite-facies activity at 2.4 Ga was suggested by Kleinschmidt and Talarico (2000) for the MSZ. However, Duclaux et al. (2008) interpreted this Neoarchean age (2.4 Ga) as being related to a regional orogenic tectonothermal event. This Neoarchean Siderian orogenic event is recorded over the entire eastern region of the Terre Adélie Craton (Ménot et al., 2005, 2007; Duclaux et al., 2008). The deformation of the Terre Adélie Craton (TAC) occurred during Neoarchean to Palaeoproterozoic times. This was a critical period in the Earth's evolution (Hamilton, 1998) which included

* Corresponding author.
E-mail address: gaelle.lamarque@univ-st-etienne.fr (G. Lamarque).

http://dx.doi.org/10.1016/j.tecto.2016.05.011
0040-1951/

the transition from Archean geodynamics, with heat loss mostly associated with massive magmatic transfer from a mantle which was much hotter than at present, to modern style geodynamics related to plate tectonics (Lee et al., 2008; Dhuime et al., 2012). The MSZ constitutes one of the oldest known shear zones preserved from the early period of modern plate tectonics through its 1.7 Ga activation. It could have been contiguous with the Kalinjala or Coorong shear zones (South Australia) before the Southern Ocean opening during the Cretaceous period (Talarico and Kleinschmidt, 2003; Gibson et al., 2013). Despite its very old age (1.7 to 1.5 Ga), MSZ activity was not associated with voluminous magma injection and differs strikingly from younger Neoproterozoic and Cambrian shear zones for example in Madagascar (Grujic and Mancktelow, 1998; Martelat et al., 1999). Other examples of shear zones from Palaeo- to Mesoproterozoic times in Colorado (Anderson and Cullers, 1999; Shaw et al., 2001), from Neoproterozoic times in South-Africa (Kisters et al., 1998), from Pan-African times in North Africa (Boullier and Bertrand, 1981), in West-Africa (Adissin Glodji et al., 2014) and in North-East Brazil (Tommasi et al., 1994; Neves and Vauchez, 1995; Neves et al., 1996, 2000), and more recently during the Cretaceous in New Zealand (Barker et al., 2010), are commonly associated with high magma production and emplacement (see Brown and Solar, 1998 for a synthesis of deformation and linked melt production).

Knowledge of the deep structures' continuity (potentially down to the mantle) allows a better understanding of the deformation distribution across the lithosphere and therefore its rheology. However, the lack of mantle-derived melt injection during the activation of the MSZ does not provide an argument for a possible continuity of the deformation down to the mantle. Structural studies show that amphibolite and retrogressed granulite are both affected by the 1.7 Ga deformation (Pelletier et al., 2002; Ménot et al., 2005; Gapais et al., 2008), but no lower crust or mantle xenoliths were found. These observations only argue that the MSZ penetrates at least down to the intermediate crust. Because of the lack of geological evidence, other tools have to be used to image the deep structure of the shear zone.

A geophysical approach can provide alternative information. SKS-wave anisotropy is an efficient tool for mapping mantle structure deformation (Silver, 1996), as SKS samples an entire vertical section through both asthenosphere and lithosphere. For the Terre Adélie and George V Land region, no clear continuation of the MSZ into the lithospheric mantle was observed from the SKS-wave anisotropy study of Lamarque et al. (2015) despite a strong variation in crustal thicknesses on both sides of the MSZ highlighted by the airborne gravity study of Jordan et al. (2013) and receiver function analysis of Lamarque et al. (2015). In order to fully interpret the seismic recordings for the MSZ, it is therefore necessary to determine the crustal contribution of the SKS-wave anisotropy measurements.

The present study focuses, firstly on the description of deformation processes based on analysis of micrometric to millimetric scale structures. It was performed by both optical analysis and electron backscatter diffraction (EBSD) crystallographic preferred orientation (CPO) measurements in samples from the strongly deformed domains of the MSZ (mylonites) and from the less affected areas outside the shear zone where numerous tectonic boudins are preserved. Subsequently, CPO measurements and modal compositions allow us to calculate the contribution of the crust, in particular the one due to the MSZ ductile deformation. Results are compared to the SKS-wave anisotropy measurements of the TAC performed by Lamarque et al. (2015).

2. Geological settings

The Mertz shear zone (MSZ) is a major structure clearly visible at the Correll Nunatak (67°35′S, 144°16′E; Stillwell, 1918; Di Vincenzo et al., 2007; Ménot et al., 2007), Fig. 1. The MSZ activation occurred during the 1.7 Ga tectono-metamorphic event (Di Vincenzo et al., 2007; Duclaux et al., 2008), synchronously with the structuration of the Dumont d'Urville and Cape Hunter sedimentary basins, the activation of the Zélée shear zone (141°E) and the development of a network of anastomosed narrow shear zones that have affected the Neoarchean basement, which is still visible at Stillwell Island for example.

The MSZ marks the boundary between the Neoarchean to Palaeoproterozoic TAC and a metasedimentary complex intruded by a 0.5 Ga-old granitic suite related to the Ross Orogeny (Fanning et al., 2002; Di Vincenzo et al., 2007).

At Correll Nunatak, the mylonitic foliation is decimetre-thick subvertical and oriented N340° to N–S. The mineral lineation is found to be gently dipping and most of shear markers clearly indicate a dextral shear sense (Kleinschmidt and Talarico, 2000; Talarico and Kleinschmidt, 2003; this study). From mineral assemblage observations, the MSZ might represent a mid-crustal strike-slip fault that could have accommodated large horizontal displacements during successive shearing events at 1.7 and 1.5 Ga in amphibolite and greenschist facies conditions, respectively (Di Vincenzo et al., 2007; Duclaux et al., 2008). However, the last activation of the MSZ at 1.5 Ga was discussed by Ménot et al. (2005), who suggested that a younger age (maybe post-Ordovician) cannot be formally ruled out because Palaeozoic rocks are found to be juxtaposed east of the MSZ.

Within the MSZ, some tectonic boudins preserve such Neoarchean penetrative structures of the TAC. They are predominantly composed of felsic to mafic orthogneiss and granite intruding metasedimentary country rocks. This 2.55–2.44 Ga old continental crustal segment (Oliver and Fanning, 2002; Duclaux et al., 2008) exposes two distinct tectonic units (Port Martin and East Commonwealth Bay) that were metamorphosed under amphibolite and granulite facies conditions respectively, and represent intermediate to deep crustal sections (Ménot et al., 2005), Fig. 1.

More detailed geological settings are presented in the Supplementary materials (Appendix 1) with a structural description of the studied outcrops.

3. Microstructures

3.1. Methods

We studied 20 samples located at Correll Nunatak in the amphibolite facies unit and at Aurora Peak, Murchison Mount, Cape Gray and Stillwell Island in the granulite domain (Fig. 1). We grouped the samples according to their deformation microstructures (strongly, moderately and weakly deformed samples) then, we selected one or two representative samples from each group.

Crystallographic orientations were measured by electron backscatter diffraction (EBSD) technique using a scanning electron microscope JEOL JSM 5600 at the University of Montpellier and a JEOL JSM 6500F at the Ecole des Mines at Saint-Etienne. Polished thin sections were made parallel to the lineation and perpendicular to the foliation (XY plane). Electron backscatter diffraction patterns (EBSPs) were acquired at an accelerating voltage of 17 kV and a working distance of about 25 mm. They were manually or automatically (step size of 10 μm) acquired and indexed using the Channel 5 software from HKL Technology, Denmark. For analysis, 5–7 Kikuchi bands were matched with expected EBSPs. The accuracy of the crystallographic orientation of each measurement is typically lesser than 1°.

Crystallographic orientations are displayed using pole figures, with equal area lower hemisphere projections, where the sample lineation is represented by X, the foliation plane is represented by (XY) and the direction normal to the foliation plane by Z. The fabric strength is quantified by using the dimensionless J-index (Bunge, 1982), which is equal to 1 for a random distribution and tends toward infinity for a single crystal orientation.

In some samples, foliation plane and lineation direction were not easy to identify. In order to replace EBSD measurements in the structural frame (X, Y, Z), we used magnetic foliation and lineation identification

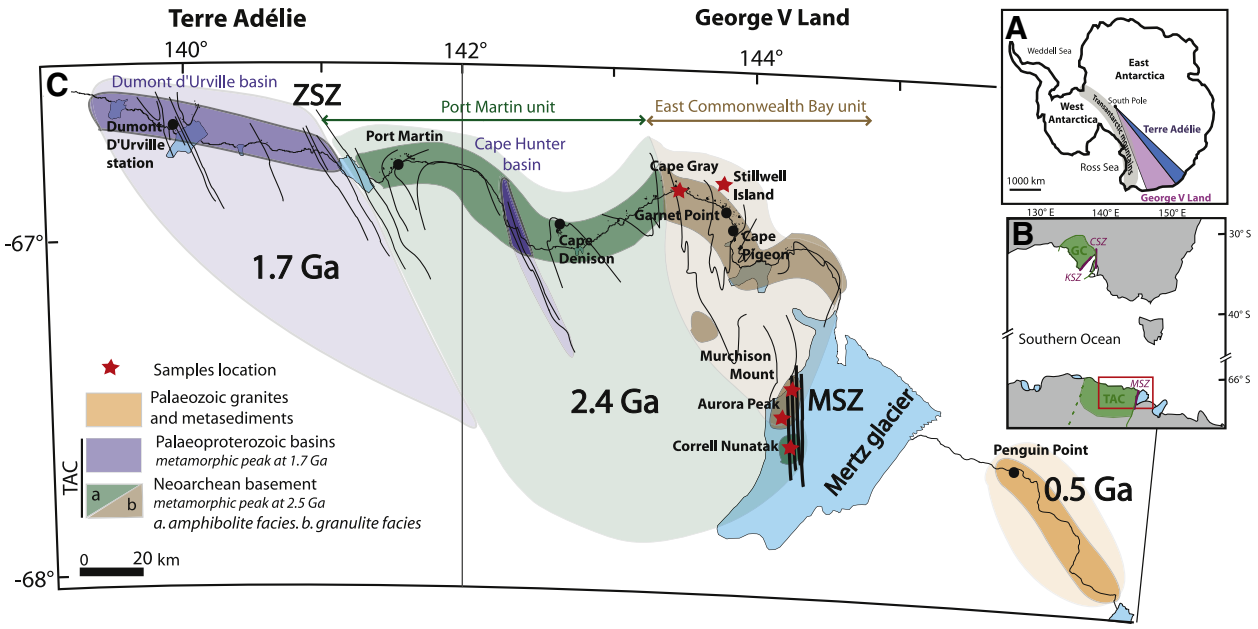

Fig. 1. A: Location of Terre Adélie and George V Land in the Antarctic continent. **B:** Link between south Australia and Antarctica. TAC = Terre Adélie Craton, GC = Gawler Craton, MSZ = Mertz shear zone, KSZ = Kalinjala shear zone, CSZ = Coorong shear zone. **C:** Synthetic geological map of the Terre Adélie Craton (after Ménot et al., 2007). Purple areas are Palaeoproterozoic terrains, which correspond to the Dumont d'Urville and Cape Hunter basins; green and brown areas are Neoarchean terrains, green being intermediate to upper amphibolitic crust and brown granulite facies crust. Orange area represents the Paleozoic crust, mainly composed of granitoids. The darkest colours correspond to outcrops. MSZ denotes the Mertz shear zone and ZSZ denotes the Zélée shear zone. Directions of field-measured structures are drawn in black. Locations of studied samples are marked by red stars. See also Ménot et al. (2007) and Ménot (to be published) for more complete geological description. (For interpretation of the references to colour in this figure legend, the reader is referred to the web version of this article.)

using anisotropy of magnetic susceptibility (AMS) technique. The AMS was measured using a MFK1 Kappabridge instrument (AGICO, Brno) at the University of Saint-Étienne (France). We evaluate the three principal susceptibility axes (K_1, K_2 and K_3 with $K_1 \geq K_2 \geq K_3$) of the AMS ellipsoid in a low-magnetic field (200 $A \cdot m^{-1}$). The K_1 and K_3 axes can be associated with the magnetic lineation and the magnetic foliation pole, respectively. We performed measurements on cubes, one of the faces being parallel to the corresponding thin section. In metamorphic rocks magnetic foliation and lineation generally correspond closely to the tectonic structures (Borradaile and Henry, 1997; Egydio-Silva et al., 2005; personal observations in mylonites from Correll) and we can thus discuss crystallographic fabrics in relation to the structural framework.

3.2. Microstructures from various rock types

We describe microstructures from both the Neoarchean granulite facies condition deformation and the Palaeoproterozoic amphibolite to greenschist facies conditions deformation related to the MSZ. To study Neoarchean deformation, we selected samples from East Commonwealth Bay (Aurora, Murchison, Stillwell, Cape Gray) where the lower crustal structure is well preserved. Four strongly deformed rocks (GD06-28 and RPM98-114 from Aurora, RPM98-101 from Murchison and RPM98-138 from Stillwell) and five moderately deformed rocks (RPM98-121, GD06-25, RPM98-122 and RPM98-126 from Aurora and RPM98-169B from Cape Gray) were also analysed. Moreover, three weakly deformed rocks were studied: two from a granulite facies preserved core at Aurora (RPM98-118 and RPM98-120) close to the MSZ, and another far from the MSZ at Cape Pigeon (RPM98-166). The MSZ Palaeoproterozoic tectonic event is studied at Correll Nunatak (Di Vincenzo et al., 2007) using six mylonite samples (RPM98-106, GD06-07, GD06-08, GD06-10, GD06-12 and GD06-16), and using sample 12-CJB-12D from a localized shear zone in the anatectic granites of Stillwell Island. Name, location and modal composition of selected samples are indicated in Table 1. Mineral abbreviations are from Whitney and Evans (2010). Modal compositions were evaluated from both automatic EBSD analyses and images analyses (photographs of thin sections). Figs. 2 and 3 show the structural context of the outcrops and photographs of corresponding thin-sections, respectively. Detailed petro-microstructural descriptions of studied samples are given in Supplementary materials (Appendix 2). We focus below on minerals for which EBSD measurements were carried out.

3.2.1. Neoarchean deformations

3.2.1.1. Strongly deformed rocks. Quartz is present as isolated grains in RPM98-114, as aggregated grains in RPM98-101 and as ribbons in GD06-28. In all samples, the grain size is about 0.05 to 0.5 mm and all crystals present irregular and lobed grain boundaries with evidence of plastic deformation (undulose extinction, for example). Feldspar grains are recrystallized with grain angles of 120° (around 0.1 to 0.3 mm in grain size) in sample GD06-28. In the two others samples, few porphyroclasts (about 0.1 mm in size) show evidence of plastic deformation whereas recrystallized grains have textural equilibrium (0.01–0.02 mm). Orthopyroxene mainly consists of recrystallized grains (around 0.05 mm) aligned along the foliation (XY) plane in sample GD06-28 whereas it is present as isolated porphyroclasts of 0.1–0.2 mm with some associated recrystallized grains in sample RPM98-114. In both samples, orthopyroxene grains do not show evidence of kinking but are slightly affected by a late amphibolitization, along fractures and cleavage. In sample RPM98-114, biotite (0.1 to 0.2 mm long) also occurs as a late recrystallization phase around orthopyroxene.

3.2.1.2. Moderately deformed rocks. Quartz grains in all samples have very irregular and lobed grain boundaries as well as marked undulose extinction. They are aggregated and tend to form polycrystalline ribbons. In some cases, they can contain small inclusion of feldspar and biotite. Feldspars are mainly present in moderately deformed samples as recrystallized grains (0.05 to 0.2 mm) with equilibrated textures. In samples RPM98-121 and RPM98-138, few porphyroclasts are preserved and show evidence of plastic deformation (undulose extinction, curved and bevelled twins). Biotite grains, when present, are mainly aligned along

Table 1
Petrology, sample name, location and modal composition (%) of the 18 selected samples (3 strongly, 3 moderately and 2 weakly deformed rocks). Opx = orthopyroxene, Pl = feldspar plagioclase, KF = K-feldspar, Ox = oxide, Bt = biotite, Qtz = quartz, Am = amphibole, Gt = garnet, Cpx = clinopyroxene, Sill = sillimanite.

Petrology	Sample name	Location	Mineralogy						
			Opx	Pl	KF	Ox	Bt	Qtz	Others
Granulite facies samples (2.4 Ga)									
Strongly deformed rocks									
Gneiss with Opx + Pl	GD06-28	Aurora	12	40	4	1	<1	43	
	RPM98-114	Aurora	5	45	5	5	<1	39	Gt < 1
Gneiss	RPM98-101	Murchison	<1	29	59	<1		12	
Moderately deformed rocks									
Granulite	RPM98-121	Aurora	<1	62	4	2	<1	31	Cpx < 1
Granulite	GD06-25	Aurora	1	32	22	1		44	
Gneiss	RPM98-122	Aurora	2	26	3	<1	3	51	Gt 14
Gneiss	RPM98-138	Stillwell		33	35	3	5	10	Sill 13
									Gt < 1
Weakly deformed rocks									
Gneiss with Opx + Pl	RPM98-118	Aurora	15	70	3	5	5	<1	Amp < 1
									Cpx < 1
	RPM98-120	Aurora	15	71	5	5	2		Amp < 1
									Cpx < 1
	RPM98-166	Cape Gray	16	66	13	3	1	<1	Amp < 1
									Cpx < 1
Amphibolite facies samples (1.7 Ga)									
Strongly deformed rocks									
Granodioritic orthogneiss	RPM98-106	Correll		27	48		<1	24	Cpx < 1
Orthogneiss	GD06-07	Correll		50	8	<1	6	15	Amp 21
	GD06-08	Correll		46	12		10	5	Amp 27
	GD06-10	Correll		39	38		6	12	Amp 5
	GD06-12	Correll		41	37		<1	1	Amp 20
	GD06-16	Correll		33	1	<1	5	6	Amp 55
	GD06-18	Correll		40	25		12	8	Amp 15
Moderately deformed rocks									
Granite	12-CJB-12D	Stillwell		21	13		8	56	Amp < 1

the foliation plane and can be measured from 0.1–0.2 mm long (sample RPM98-121) to 1.0–1.2 mm long (sample RPM98-122). Orthopyroxene is present in sample GD06-25 as grains about 1 mm aligned along the foliation (XY) plane, and in sample RPM98-122 as isolated grains of 0.1–0.2 mm with no evidence of kinking and with texturally equilibrated grain boundaries.

3.2.1.3. Weakly deformed rocks. Orthopyroxene grains are rounded with a grain size of 0.5–2.0 mm. They do not present evidence of kinking nor alteration although they are fractured. They occur as isolated grains or as cluster of 4–5 grains generally aligned along the foliation (XY) plane. Late-stage biotite and quartz symplectites are concentrated around orthopyroxene grains or along their fractures. These biotite grains are not aligned along the foliation (XY) plane as their crystallization from orthopyroxene grains occurred after the 2.4 Ga granulite tectonic event. Plagioclase grains are bigger than the ones in strongly and moderately deformed samples (about 1 mm). The polygonal grain boundaries, with angles around 120°, suggest a large degree of recrystallization. In samples RPM98-166 and RPM98-118 we clearly distinguish two generations of plagioclase: the first one is represented by the porphyroclasts and the second one by the neoblasts. In sample RPM98-166 plagioclase neoblasts are in textural equilibrium but some porphyroclasts present irregular grain boundaries and bevelled twins, suggesting plastic deformation. Plagioclase porphyroclasts from sample

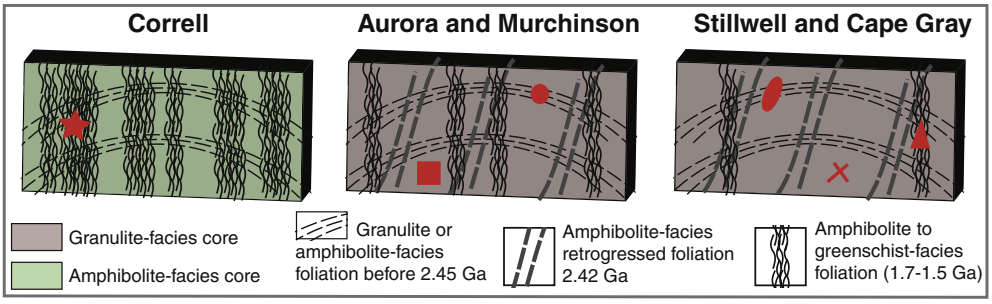

Fig. 2. Vertical cross-sections of outcrops from Correll, Aurora and Murchison, Stillwell and Cape Gray. We distinguish: 1/ the granulite-facies (Aurora Peak, Stillwell Island and Cape Gray) and amphibolite-facies (Correll Nunatak) cores formed at 2.8–2.6 Ga, which constitute the weakly deformed rocks, 2/ the preserved granulite-facies or amphibolite-facies foliation imprinted between 2.6 and 2.45 Ga, 3/ the amphibolite-facies foliation associated with the retrogression in the lower and intermediate crust at 2.45 Ga. This deformation is associated with the development of the dome-basin structures. At Correll Nunatak, this deformation could have been entirely reworked during the MSZ activation, 4/ the amphibolite to greenschist-facies conditions of deformation occurring between 1.7 and 1.5 Ga, related to the MSZ. Red symbols refer to samples presented in Fig. 3: stars and triangles correspond to 1.7 Ga amphibolite deformation at Correll (samples RPM98-106, GD06-07, GD06-08, GD06-10, GD06-12, GD06-16, GD06-18) and Stillwell (sample 12-CJB-12D) respectively, circles and ellipses correspond to granulite deformation prior to 2.45 Ga at Aurora (samples GD06-28, RPM98-114, RPM98-101, RPM98-121, GD06-25, RPM98-122) and at Stillwell (sample RPM98-138) respectively, cross and squares correspond to granulite core at Cape Gray (sample RPM98-166) and at Aurora (samples RPM98-120 and RPM98-118) respectively. (For interpretation of the references to colour in this figure legend, the reader is referred to the web version of this article.)

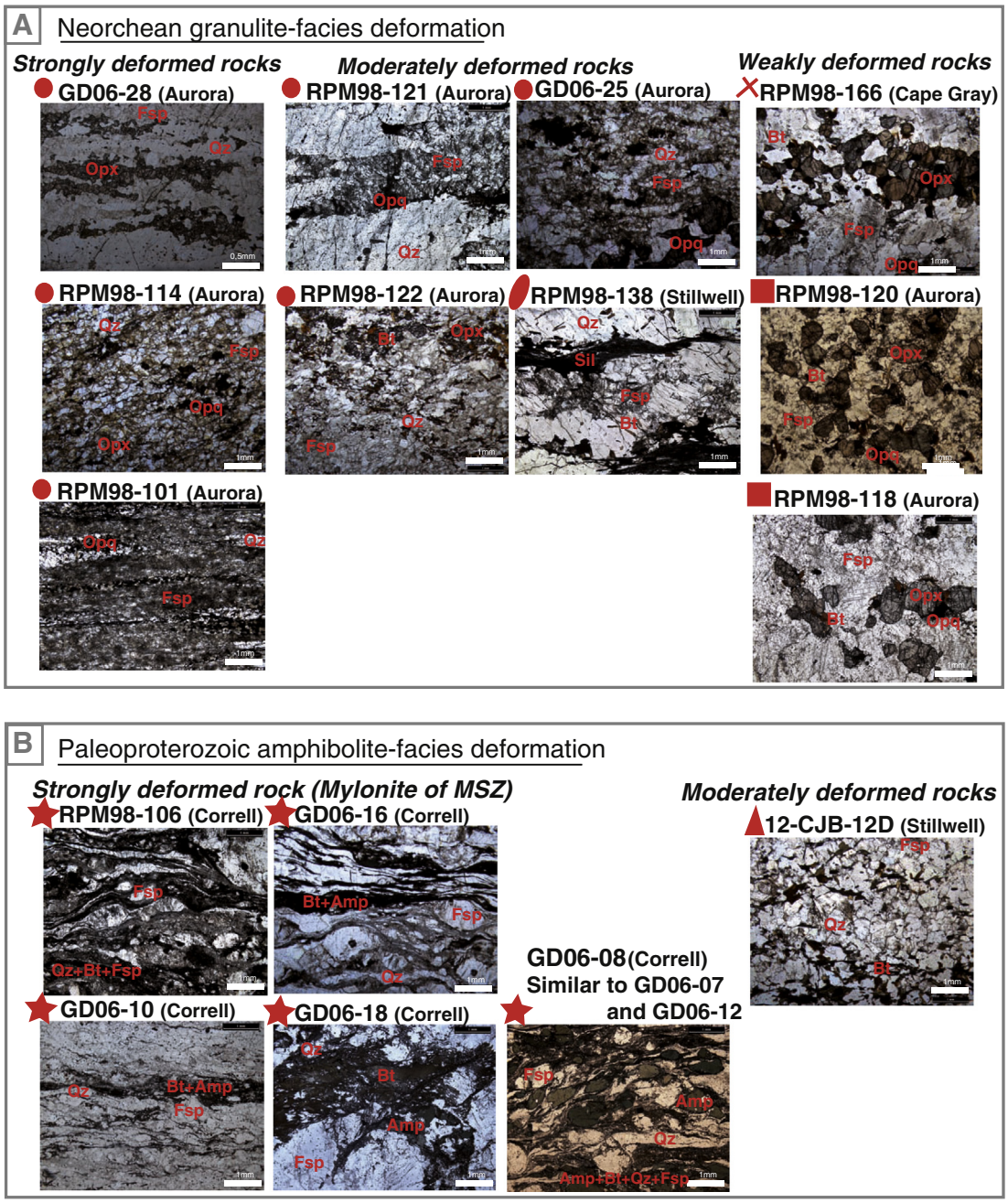

Fig. 3. A/ Photographs of the Neoarchean granulite-facies thin-sections. B/ Photographs of the Palaeoproterozoic amphibolite-facies thin-sections. See Fig. 2 for structural context.

RPM98-118 show little evidence of plastic deformation. Lastly, sample RPM98-120 contains only a few recrystallized grains and the plagioclase porphyroclasts do not show plastic deformation structures.

3.2.2. Palaeoproterozoic deformation

3.2.2.1. Strongly deformed rocks: mylonites from the MSZ. All samples are characterized by coexisting large porphyroclasts and mylonitic bands of highly deformed minerals. Porphyroclasts are mainly K-feldspar grains (microclines) with undulose extinction and around 1 mm in size. Some porphyroclasts are made of plagioclase and amphibole grains and assemblages of quartz, feldspar and biotite replace others. Fine grains (less than 0.1 mm) of biotite, amphibole, plagioclase and quartz constitute deformation bands around the porphyroclasts and define the foliation. Quartz forms irregular ribbons showing evidence of grain boundary migration such as lobed edges and/or plastic deformation (undulose extinction) depending on the sample.

The microstructure of sample GD06-18 slightly differs with the foliation defined by biotite alignment (0.3 to 1 mm long). Quartz is aggregated in areas containing porphyroclasts (about 0.3 mm) and neoblasts (0.05 mm) formed by dynamic recrystallization (subgrain rotation).

3.2.2.2. Moderately deformed rock: localized shear zone. The deformation is mainly localized into shear bands composed of biotite and small neoblast grains of quartz and feldspar (less than 0.2 mm). Biotite grains are mainly aligned along the foliation (XY) plane but another direction at 45° is also observed (SC structures). Bands of larger quartz and feldspar grains (0.3–0.5 mm) are characterized by partial recrystallization with equilibrated structures (120° angles) for feldspar. The recrystallization was not complete as some grain boundaries are irregular.

3.3. Crystallographic preferred orientations

3.3.1. Quartz

The quartz CPOs are presented in Fig. 4. First, we present results of quartz CPO from samples collected in the Neoarchean granulite facies tectonic boudins. The fabric strength of GD06-28 (Jindex = 4.9) is significantly higher than for other samples (Jindex <3.5). The quartz CPOs of sample GD06-28 are characterized by [11–20]-axes ([a]-axes) oriented in a girdle in the (XZ) plane with a stronger concentration at about 25° to the lineation X-axis. The [0001]-axes ([c]-axes) tend to form a girdle along a plane that passes through the Y-axis, at an angle of 30° to the (XZ) plane. The maximum concentration of [0001]-axes is clearly defined close to Y. The axis distribution characteristics of samples RPM98-114 and RPM98-101 are close to those of sample GD06-28, with [11–20]-axes oriented in a girdle in the (XZ) plane with the maximum concentration close to the lineation X-axis and [0001]-axes with two point maxima, the most concentrated close to the Y-axis, and the second one oriented at about 30° to the Z-axis. Moderately deformed sample RPM98-121 has the quartz [11–20]-axes oriented close to the lineation and the c-axes oriented in a girdle in the YZ plane. The maximum concentration of [0001]-axes in this sample is at 20° to the Z-axis. Moderately deformed quartz [0001]-axes of the Neoarchean sample GD06-25 form an incomplete and asymmetric cross girdle with an opening angle about 90°. The maximum concentration of [11–20]-axes is extremely low, oriented at around 10° to the lineation. Quartz fabrics from the moderately deformed samples RPM98-122 and RPM98-138 are very weak. The [0001]-axes are in a girdle around the (XY) plane with maximum concentration at 30° to the X-axis, and weakly clustered around the Y-axis, respectively. The [11–20]-axes do not have a clear orientation.

All the mylonite samples from the 1.7 Ga amphibolite event present a similar quartz CPO, except for sample GD06-18. The [0001]-axes are mainly in girdle around the (YZ) plane with maximum concentrations ranging between 3 and 5. The maximum concentrations are located close to the Y-axis for samples GD06-07, GD06-08 and GD06-12, and at 20 to 40° from the Y-axis in samples RPM98-106, GD06-10 and GD06-12. The [11–20]-axes are in a girdle around the (XZ) plane for all these samples, with maximum concentrations oriented at a low angle to the X-axis (from 0 to 30°). In sample GD06-16, the concentration of [11–20]-axes is extremely weak. Samples GD06-08 and GD06-10 have [0001]-axes more concentrated around the Y-axis than the other samples. Sample GD06-18 has a different quartz CPO, with [0001]-axes oriented parallel to the Z-axis and [11–20]-axes parallel to the X-axis. Finally, sample 12-CJB-12D, which was moderately deformed during the Palaeoproterozoic amphibolite facies tectonic event, shows poorly concentrated [0001]-axes (maximum density < 3) in a girdle at 30–50° angle to the foliation plane, with a maximum at 30° to the Y-axis. The [11–20]-axes tend to be oriented in a girdle around the (XZ) plane but the maximum density is low and the fabric is weak.

3.3.2. Feldspar

Feldspar constitutes the main phase (from 30 to 70%) of all studied samples and plagioclase is more abundant than K-feldspar. We present the CPO for plagioclase in Fig. 5. They are low, almost isotropic, with maximal density from 1.79 to 2.97.

In the Neoarchean domain, all strongly and moderately deformed granulite facies samples display quasi-isotropic feldspar fabrics (Fig. 5). The maximum concentration (M.D.) of [100]-axes, (010)-poles and (001)-poles ranges from 2.1 to 2.5 with no clear relation to the structural framework. Samples with the clearest feldspar CPO in relation to the structural framework are RPM98-118, RPM98-120 and RPM98-166 from the weakly deformed group. In these samples, poles of (010) are parallel to the magnetic foliation pole and [100]-axes are parallel to the magnetic lineation. The (001)-poles are not clearly oriented in relation to the structural framework.

In samples deformed at 1.7 Ga under amphibolite facies conditions, feldspar CPOs are also extremely low and show no clear relation to

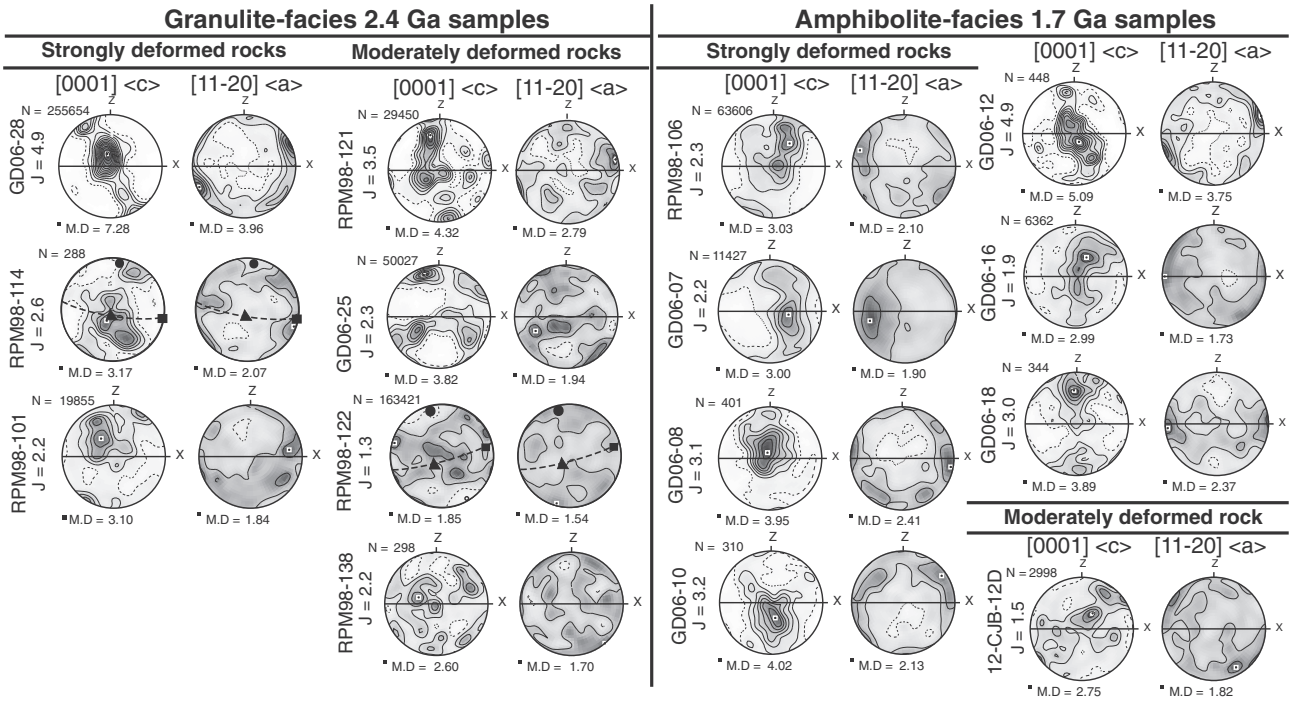

Fig. 4. Quartz CPOs are shown for strongly and moderately deformed samples in both 2.4 Ga granulite-facies and 1.7 Ga amphibolite-facies. CPOs are represented on equal area, lower hemisphere projections. Foliation is marked by a black line when clearly observed and by a dashed line when the plane was less clear. Lineation, when determined, is marked by the structural axis X. When foliation and lineation were not identifiable, measurements of magnetic foliation and lineation were carried out. Square, triangle and circle represent K1 (magnetic lineation), K2 and K3 (pole of magnetic foliation) respectively. The density contours are from 0.5 (dashed line) to the maximum density at intervals of 0.5. N is the number of measurements and M.D. the maximum density represented by a small square.

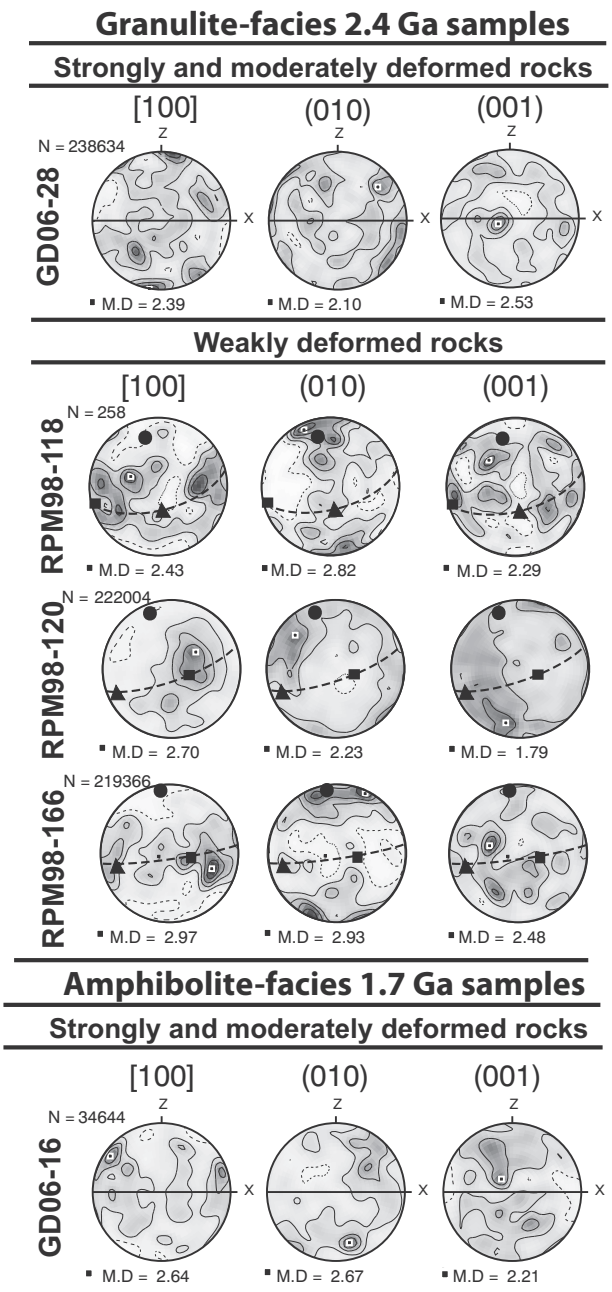

Fig. 5. Plagioclase CPOs are shown for strongly and moderately deformed samples in both 2.4 Ga granulite-facies and 1.7 Ga amphibolite-facies. CPOs are represented on equal area, lower hemisphere projections. Foliation is marked by a black line when clearly observed and by a dashed line when the plane was less clear. Lineation, when determined, is marked by the structural axis X. When foliation and lineation were not identifiable, measurements of magnetic foliation and lineation were carried out. Square, triangle and circle represent K1 (magnetic lineation), K2 and K3 (pole of magnetic foliation) respectively. The density contours are from 0.5 (dashed line) to the maximum density at intervals of 0.5. N is the number of measurements and M.D. the maximum density represented by a small square.

the tectonic foliation. GD06-16 is the sample with the most clearly defined feldspar CPO. It presents a density maximum of (010)-poles parallel to the foliation plane and [100]-axes parallel to the lineation.

3.3.3. Biotite and amphibole

The CPOs for biotite and amphibole are displayed in Fig. 6. The biotite crystal CPOs were measured in the Neoarchean domain for the moderately deformed samples RPM98-122 and RPM98-138 and for the weakly deformed samples RPM98-166 and RPM98-120. In the amphibolite facies samples from Palaeoproterozoic shear zones, strongly deformed samples GD06-07 and GD06-16 as well as moderately deformed sample 12-CJB-12D are all biotite-bearing. In both granulite and amphibolite facies domains, strongly and moderately deformed samples present clear biotite fabrics, with [001]-axes ([c]-axes) clustering more strongly than the other crystallographic axes and oriented perpendicular to the foliation. Axes [100] and [110] tend to be oriented in a girdle in the foliation plane. The biotite CPOs from weakly deformed samples present different patterns. Sample RPM98-166 shows biotite [001]-axes concentrated in a two point maxima oriented at a high angle to the foliation and lineation. Sample RPM98-120 shows biotite [100]-axes close to the magnetic lineation, [110]-axes oriented at 30° to the magnetic foliation and [001]-axes that tend to be close to the magnetic K2 (Y-axis), i.e. perpendicular to magnetic lineation and within the magnetic foliation plane.

Amphibole is only present in the Palaeoproterozoic amphibolitic mylonites. We measured the amphibole CPO in strongly deformed samples GD06-07, GD06-08, GD06-12 and GD06-16. For all samples, the [001]-axes are parallel to the stretching lineation. In sample GD06-07, both (100) and (010) tend to be oriented parallel to the foliation. In sample GD06-08, amphibole (100) is oriented parallel to the foliation. In samples GD06-12 and GD06-16, (100) for amphibole presents two maxima close to Y and Z. In all four samples, maximum densities are higher for (100)- than for (010)-poles.

3.3.4. Orthopyroxene

Orthopyroxene is a main phase in granulite rocks but is not present in amphibolites from the 1.7 Ga shear zones. The CPOs for orthopyroxene are displayed in Fig. 7. Strongly deformed Neoarchean samples GD06-28 and RPM98-114 show a preferred orthopyroxene orientation characterized by (100) oriented parallel to the foliation plane, [001] parallel to the stretching lineation and clustering of [010] near the Y structural direction. Others samples have different fabrics. The moderately deformed sample GD06-25 shows a preferred orientation of orthopyroxene with (010) oriented parallel to the foliation plane, [100]-axes parallel to the stretching lineation and [001]-axes oriented in the foliation plane with two density maxima close to the Y-axis. The orthopyroxene CPOs for the moderately deformed sample RPM98-122 are very interesting: [001] is clearly parallel to the stretching lineation, but both (100)- and (010)-poles have concentrations perpendicular to the foliation plane. Weakly deformed RPM98-166 and RPM98-120 samples show a clear preferred orthopyroxene orientation with (010) oriented parallel to the foliation plane, [001]-axes parallel to the stretching lineation and clustering of [100]-axes near the Y structural direction. The last weakly deformed sample RPM98-118 has orthopyroxene (010) oriented parallel to the foliation, as in the other weakly deformed samples. However, [001]-axes are oriented in a girdle in the foliation plane with a maximum density close to the K2 magnetic axis (Y-axis). Orthopyroxene [100]-axes do not show any orientation with respect to the magnetic framework.

4. Seismic properties of the crust affected by the MSZ

4.1. Methods of modelling

In order to evaluate the impact of the crystallographic preferred orientation of deformed minerals on seismic anisotropy in the deep continental crust, we computed seismic properties of amphibolite and granulite facies rocks from the TAC. Computations were performed using the single crystal elastic stiffness matrix, the CPO of the main minerals and density using the Mainprice (1990) software through the Voigt–Reuss–Hill averaging system. Input parameters are as follows:

(1) Mineral proportions and compositions of amphibolite and granulite facies rocks of the TAC were estimated from thin sections using automatic EBSD mapping, image analysis, and calculations from microprobe data on minerals and based on whole-rock

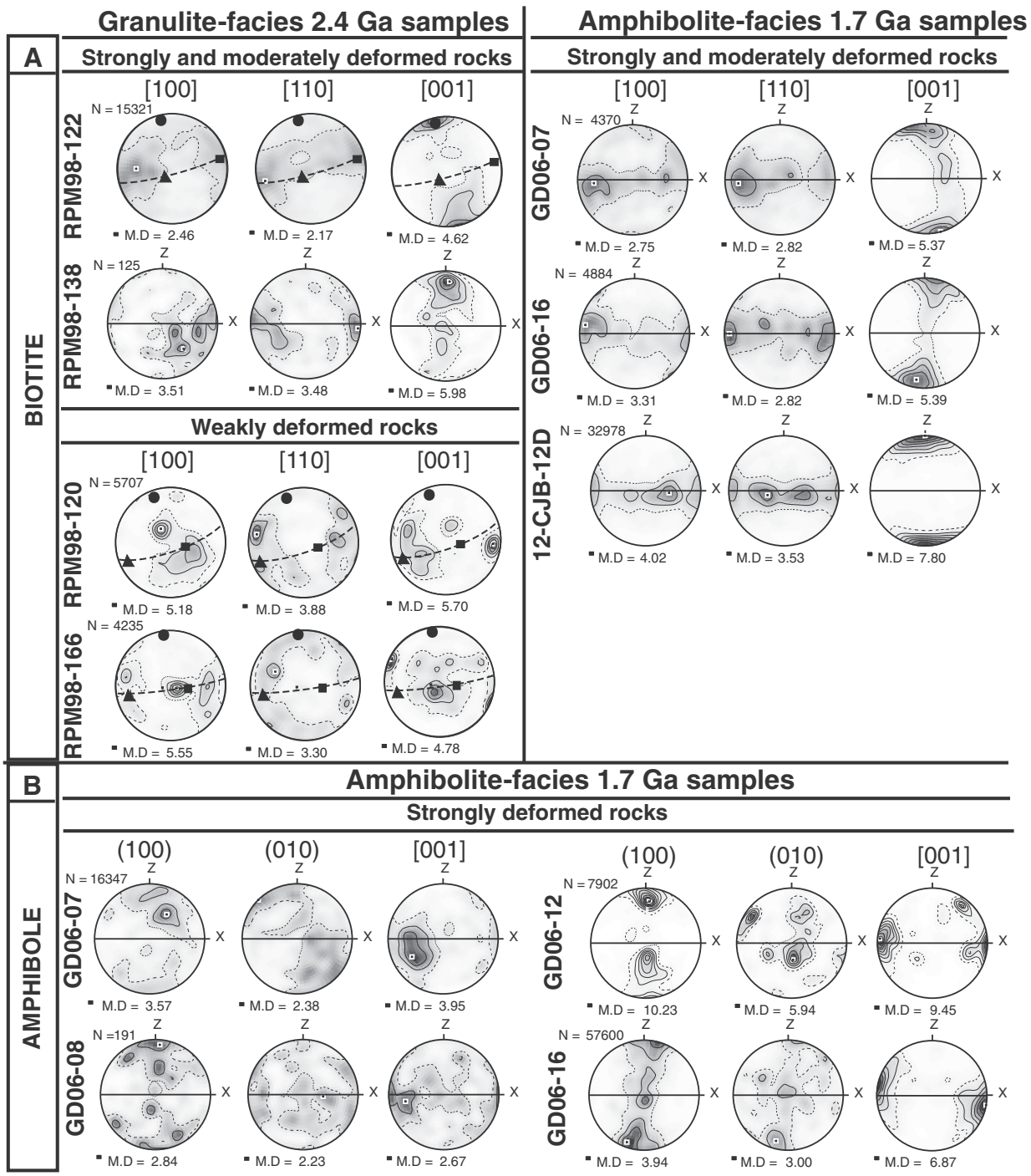

Fig. 6. Biotite and amphibole CPOs for strongly, moderately and weakly deformed samples in both 2.4 Ga granulite-facies and 1.7 Ga amphibolite-facies. CPOs are represented on equal area, lower hemisphere projections. Foliation is marked by a black line when clearly observed and by a dashed line when the plane was less clear. Lineation, when determined, is marked by the structural axis X. When foliation and lineation were not identifiable, measurements of magnetic foliation and lineation were done. Square, triangle and circle represent K1 (magnetic lineation), K2 and K3 (pole of magnetic foliation) respectively. The density contours are from 1 (dashed line) to the maximum density at intervals of 1. N is the number of measurements and M.D. the maximum density represented by a small square.

chemistry. Modal abundance was estimated from the 18 studied samples, with corroboration from previous estimations from field, microstructural and geochemical studies (Pelletier, 2001). Mineral proportions are detailed in the Supplementary material (appendix 3).

(2) EBSD-measured CPO of representative minerals from strongly and moderately deformed samples. CPO for feldspar is from sample RPM98-120, for quartz is from RPM98-114, for amphibole from GD06-16, for biotite CPO from RPM98-122 and for orthopyroxene from GD06-28, based on the commonly found (100)[001] fabric. Spinel, garnet, clinopyroxene, sillimanite and cordierite were considered as being isotropic.

(3) Single crystal elastic constants and density data for hypersthene were calculated from data in Bass and Weidner (1984) and Weidner et al. (1978). Other crystal elastic constants are taken from Aleksandrov et al. (1974) for plagioclase, McSkimin et al. (1965) for quartz, Aleksandrov and Ryzhova (1961) for amphibole and biotite, Li et al. (1995) for oxide (spinel), Babuska et al. (1978)

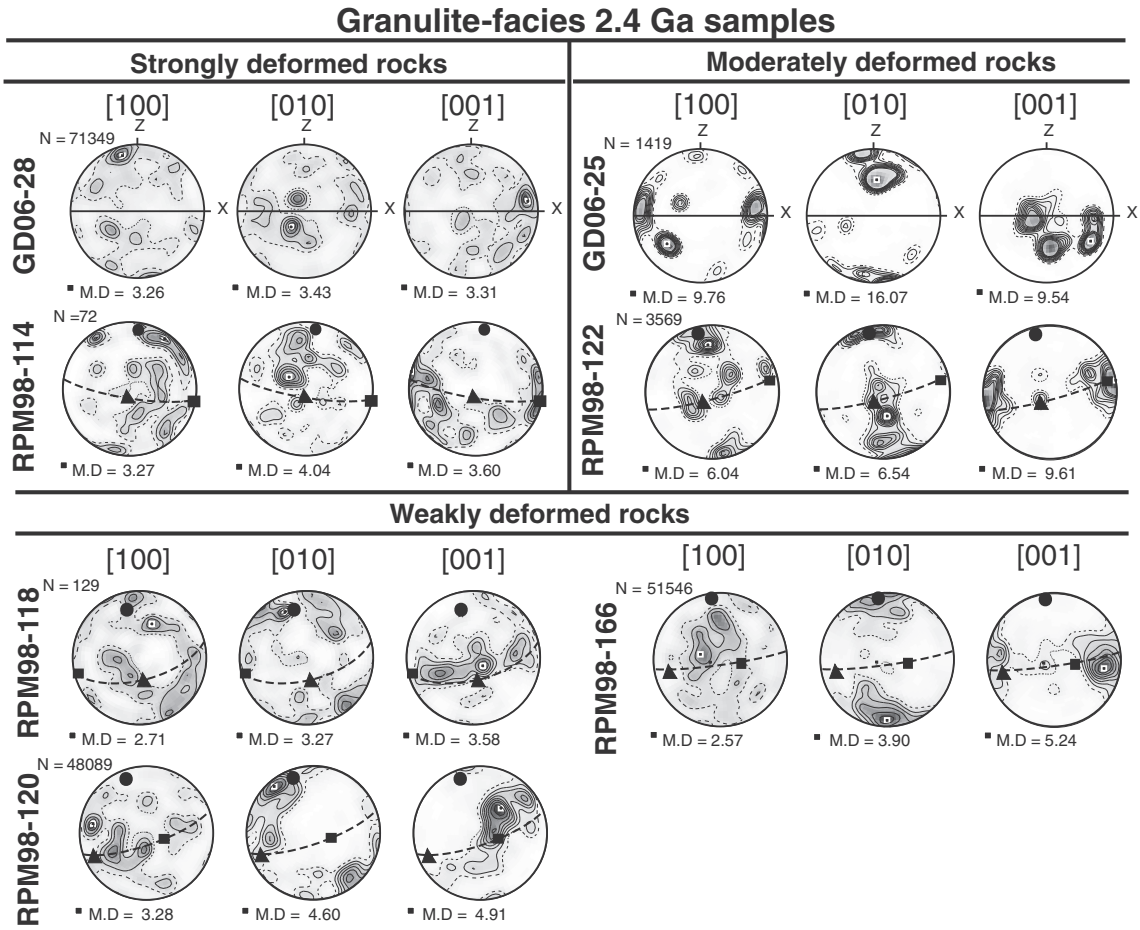

Fig. 7. Orthopyroxene CPO for strongly, moderately and weakly deformed samples in 2.4 Ga granulite-facies. CPOs are represented on equal area, lower hemisphere projections. Foliation is marked by a black line when clearly observed and by a dashed line when the plane was less clear. Lineation, when determined, is marked by the structural axis X. When foliation and lineation were not identifiable, measurements of magnetic foliation and lineation were done. Square, triangle and circle represent K1 (magnetic lineation), K2 and K3 (pole of magnetic foliation) respectively. The density contours are from 1 (dashed line) to the maximum density at intervals of 0.5. N is the number of measurements and M.D. the maximum density represented by a small square.

for garnet, Collins and Brown (1998) for clinopyroxene, Vaughan and Weidner (1978) for sillimanite and Haussühl et al. (2011) for cordierite.

4.2. Results

P-wave velocities, P- and S-wave anisotropy and the orientation of the fast S-wave polarization plane are presented in Fig. 8. Firstly we show results for various aggregates composed of 100% plagioclase, 100% quartz, 100% amphibole, 100% biotite and 100% orthopyroxene and then for the amphibolite and granulite facies, taking into account the rocks types and modal contents described in the Supplementary materials (Appendix 3).

For the plagioclase aggregate, the P-wave anisotropy is low (2.9%). The maximum of P-wave velocity is close to the perpendicular to the foliation ($Vp_{max} = 6.7$ km·s^{-1}) and the minimum of the P-wave velocity is parallel to the lineation ($Vp_{min} = 6.5$ km·s^{-1}). The maximum S-wave anisotropy is also very low (1.6%) and close to 0 in the case of an S-wave propagating parallel to Y. For the quartz aggregate, the P-wave anisotropy is relatively strong (6.3%) and the slowest (5.9 km·s^{-1}) direction of propagation is close to the structural axe Y. The maximum S-wave anisotropy is 6.6% and tends to 3.0% close to the structural axe Y. For S-waves propagating parallel to the structural axe Y, the V_{S1} polarization planes describe an angle of about 20° to the foliation. Amphibole aggregate shows strong P-wave anisotropy (11.4%), with the lowest velocity of about 6.5 km·s^{-1} perpendicular to the foliation and the highest velocity of about 7.3 km·s^{-1} parallel to lineation. The maximum S-wave anisotropy is very high (6.9%) and greater than 5.0% for an S-wave propagating parallel to the Y-axis. The polarization planes of the speed velocity waves (Vs_1) are oriented parallel to the foliation. For the biotite aggregate, the P-wave anisotropy is remarkably strong, about 21% with a velocity of 5.4 km·s^{-1} for a P-wave propagating parallel to Y. The maximum S-wave anisotropy is also the strongest one (21.1%) and it is maximal for an S-wave propagating parallel to Y. The orientation of the fast S-wave polarization plane shows a low angle to the foliation plane. Finally, the orthopyroxene aggregate shows a low P-wave anisotropy (1.4%) with a velocity of 7.3 km·s^{-1} for a P-wave propagating parallel to Y. The maximum S-wave anisotropy is also low (1.5%) and close to 0 for an S-wave propagating parallel to Y.

Fig. 8. Representative patterns of calculated seismic properties of the TAC crust affected by the MSZ. Equal area, lower hemisphere projections in X, Y, Z framework. Solid red line: foliation (XY plane) is vertical and lineation (X) is horizontal in the foliation plane. The seismic properties are: P-wave velocity (Vp, km·s^{-1}), S-wave anisotropy (AVs %) defined for a specific direction as $100 * (Vs_1 - Vs_2) / [(Vs_1 + Vs_2) / 2]$ where Vs_1 and Vs_2 are the fast and slow S-wave velocities, respectively, and the direction of the Vs_1 polarization planes. (For interpretation of the references to colour in this figure legend, the reader is referred to the web version of this article.)

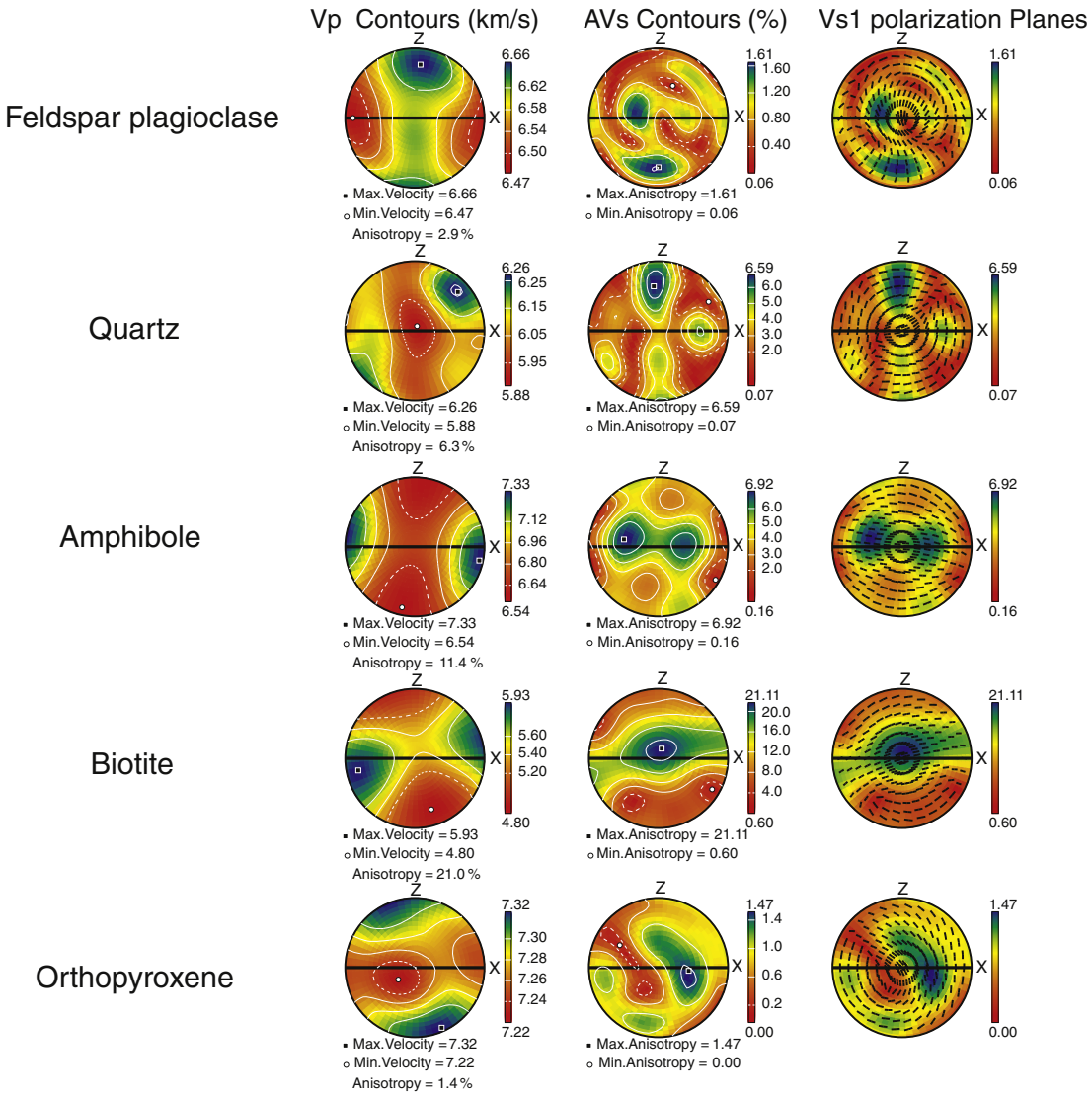

Terre Adélie amphibolite facies

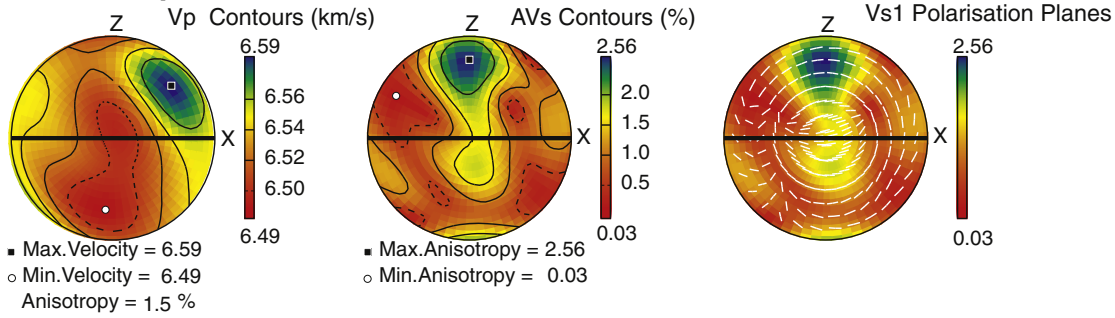

Terre Adélie granulite facies

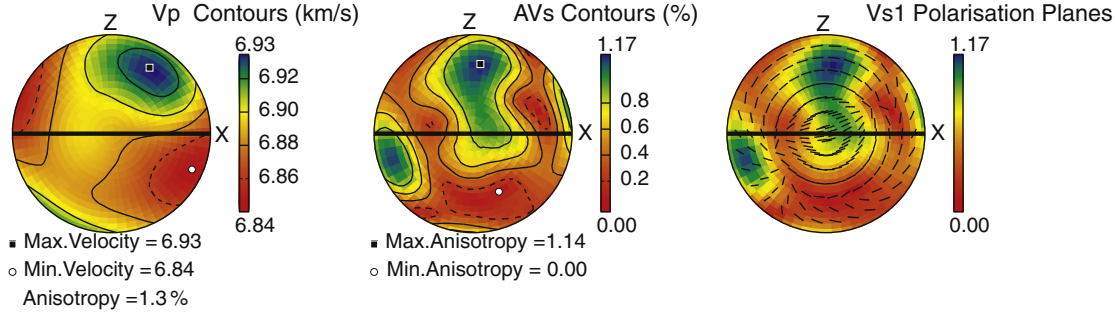

We also modelled a representative granulite and amphibolite facies crust for the Terre Adélie craton (Fig. 8) from modal proportions estimated (see Supplementary material Appendix 3 for details). It appears that the P-wave anisotropy (1.3% for granulite and 1.5% for amphibolite) and maximum S-wave anisotropy (1.1% for granulite and 2.6% for amphibolite) are low. The anisotropy of the granulite domain is less than 1% and the anisotropy of the amphibolite terrain is about 1.5% for S-waves propagating parallel to Y (i.e. propagating vertically in the displayed projection considering a foliation with a vertical dip).

5. Discussion

5.1. Deformation mechanisms from microstructure observation and CPO analysis

5.1.1. Quartz

We can distinguish four main quartz fabric patterns related to the intensity and the pressure–temperature conditions of deformation: (1) the Neoarchean granulite-facies mylonites, (2) the moderately deformed Neoarchean granulite rocks, (3) the Palaeoproterozoic amphibolite facies mylonites, and (4) the moderately deformed Palaeoproterozoic rocks.

Quartz microstructures from the Neoarchean granulite facies mylonites (samples GD06-28, RPM98-114 and RPM98-101) are characterized by undulose extinction and irregular and lobed grain boundaries related to subgrain rotation recrystallization (SGR) and grain boundary migration (GBM) occurring during plastic deformation. Passchier and Trouw (1996) defined the subgrain rotation recrystallization as the increase in angle between the crystal lattice on either side of the subgrain boundary until the subgrain forms a new grain. The authors defined the GBM high temperature process as the "increase in grain boundary mobility to an extent that grain boundaries can sweep through entire crystals to remove dislocations and possibly subgrain boundary". In the Neoarchean granulite mylonites, the [0001] and [11–20]-axis patterns in these three samples are typical of quartz CPO resulting from the dominant activation of prismatic <a> and basal <a> slip systems, with a contribution of a rhomboidal <a> slip system only in samples RPM98-101 and RPM98-114. Activation of the prismatic <a> with subordinate rhomboidal <a> slip systems is commonly interpreted as a medium to high temperature deformation (Wenk et al., 1989; Wenk and Christie, 1991; Passchier and Trouw, 1996; Menegon et al., 2008; Pennacchioni et al., 2010). However, the activation of a basal <a> slip system is interpreted as lower temperature deformation (Passchier and Trouw, 1996), and could be related to the retrogression event that occurred at about 2.42 Ga in the granulite domain (Duclaux et al., 2008). In that case, the prismatic <a> slip system would have been preserved in quartz during retrogression. This has been already identified by Toy et al. (2008) in the quartz fabrics from the Alpine Fault mylonites. The authors showed that the dominant activation of the prismatic <a> slip system during the deformation prevents an easy basal <a> slip. In that case, the prismatic <a> slip system will be largely preserved. Moreover, the strongly deformed granulite-facies sample GD06-28 shows a quartz CPO characterized by a higher concentration of [0001]-axes close to the Y-axis than the other samples. It could indicate that the prismatic <a> slip system has been more strongly activated in this sample than in samples RPM98-114 and RPM98-101. This quartz CPO is also related to a specific microstructure characterized by well-defined ribbons and more evidence of GBM processes such as lobed grain boundaries, variable grain size, and grain boundary mobility structures. This is interpreted by Jessell and Lister (1990) and Stipp et al. (2002b) as being related to an increase in deformation temperature, but could also be related to a decreasing strain rate at constant temperature (Stipp et al., 2002a; Law, 2014).

The quartz microstructures of moderately deformed granulite-facies samples are characterized by grains showing evidence of SGR and GBM. However, in contrast to the strongly deformed granulite-facies samples, grain ribbon formation is not complete in moderately deformed samples. The [0001]-axis cross girdles and [11–20]-axis patterns in the quartz are representative of the activation of prismatic <a>, rhomboidal <a> and basal <a> slip systems (Menegon et al., 2008; Augenstein and Burg, 2011) at medium temperature (Stipp et al., 2002b). The symmetry of the quartz [0001]-axis cross girdles in these samples could indicate a co-axial (pure shear) deformation (Law, 1990). Moreover, the low maximum density of these quartz CPOs, in particular for sample RPM98-122, may be related to a notable recrystallization imprint during retrogression as shown by Toy et al. (2008) for samples close to the Alpine fault.

Palaeoproterozoic amphibolite-facies mylonites display SGR and GBM microstructures associated with the [0001] and [11–20] partial girdle patterns for all samples except GD08-18. These patterns suggest the activation of both prismatic <a> and rhomboidal <a> slip systems. Similar fabrics were measured by Pennacchioni et al. (2010) in quartz veins deformed at medium temperature. The stronger concentration of [0001]-axes around the Y-axis reveals a more intense activation of the prismatic <a> slip system in samples GD06-08 and GD06-10, related to a higher temperature (Egydio-Silva et al., 2002) or a lower strain rate deformation (Stipp et al., 2002a; Law, 2014). The asymmetry of the [0001]-axes single girdle observed in these samples was predicted by Etchecopar (1977) in models of two-dimensional simple shear deformation. Sample GD06-18 differs from the other amphibolite-facies mylonites. Microstructural observations indicate that for this sample recrystallization is dominated by SGR processes. In addition, its CPO is typical of the activation of a (0001)[11–20] slip system, usually developed during lower temperature deformation (Stipp et al., 2002b; Peternell et al., 2010; Law, 2014). A low temperature deformation could be related to the very localized activation of the shear zone that could occur in green-schist-facies at 1.5 Ga, as shown by Di Vincenzo et al. (2007) and Duclaux et al. (2008) from 40Ar/39Ar dating on biotite.

Finally, the moderately deformed Palaeoproterozoic amphibolite-facies rocks display recrystallization microstructures associating SGR and GBM processes and CPO characterized by the [0001]-axes that form single girdle patterns suggesting the activation of associated prismatic <a>, rhomboidal <a> and basal <a> slip systems. As for the amphibolite-facies mylonites, the asymmetry of the [0001]-axis girdle is probably related to dominant shear strain but the development of a basal <a> slip system suggests a lower temperature of deformation.

Quartz fabrics are sensitive to temperature conditions during deformation but they do not constitute a good quantitative thermometer, as they are also sensitive to water-content (Mainprice and Paterson, 1984; Tullis and Yund, 1989; Nakashima et al., 1995; Mancktelow and Pennacchioni, 2004), water fugacity (Kronenberg and Tullis, 1984; Post et al., 1996; Chernak et al., 2009; Holyoke and Kronenberg, 2013), strain rate (Tullis et al., 1973) and strain regime (Schmid and Casey, 1986; Toy et al., 2008) see also Law (2014) and references therein for a review. However, we clearly distinguish two different tectonic events in the granulite-facies and amphibolites-facies rocks respectively, with contrasting microstructures and CPO for the two quartz populations. The activation of a basal <a> slip system in strongly deformed granulite-facies samples could be related to the retrogression event. In sample GD06-28, the preservation of a quartz CPO suggesting the activation of prismatic <a> slip system despite the recrystallization during the retrogression suggests a strong activation of this slip system during the peak metamorphic deformation. In addition, the symmetrical patterns observed for quartz CPO of moderately deformed granulite-facies samples suggest that they have recorded co-axial deformation. The amphibolite-facies rocks at Correll Nunatak were deformed during Palaeoproterozoic times by predominantly simple shear deformation. These results suggest than the quartz CPO patterns from Neoarchean boudins were preserved in spite of further deformation during Palaeoproterozoic times.

5.1.2. Feldspar

Optical microstructure analysis reveals strong evidence of plastic deformation (undulose extinction, fine curved planes) in porphyroclasts embedded in large areas of recrystallized grains. Pervasive grain boundary migration and grain growth suggest deformation mechanisms combining diffusion and dislocation creep. Such mechanisms are described for syn- to post-kinematic deformation at high temperature conditions (Egydio-Silva et al., 2002). However, fabrics measured in the present study display an extremely weak maximum concentration of axes (M.D. < 3). This lack of strong fabric can be interpreted in different ways: (1) the activation of diffusion creep in association with dislocation creep due to deformation at high temperature (Lapworth et al., 2002; Rosenberg and Stünitz, 2003), (2) grain boundary diffusion creep facilitated by significant grain size reduction during dynamic recrystallization (Jiang et al., 2000; Mehl and Hirth, 2008; Raimbourg et al., 2008; Svahnberg and Piazolo, 2010; Ji et al., 2014), and (3) simultaneous activation of several slip systems facilitated under high temperature conditions (Gandais and Willaime, 1984; Zhang et al., 1994). Interestingly, the samples that show the clearest fabric are from the weakly deformed areas (RPM98-166, RPM98-120 and RPM98-118). According to previous hypotheses, the fact that these samples present the clearest fabric could be due to a lower temperature of deformation or to the absence (or quasi-absence) of grain size reduction during dynamic recrystallization. Equilibrated microstructures marked by few undulose extinctions, few or no neoblasts and grain boundaries with angles oriented at 120° do not argue for a low temperature deformation but suggest a high degree of static recrystallization or a magmatic flow texture overprinted by incipient high temperature plastic deformation, as suggested by previous studies (Benn and Allard, 1989; Satsukawa et al., 2013; Ji et al., 2014). This CPO pattern with (010)-planes parallel to the foliation and [100]-axes parallel to the lineation has been documented in naturally deformed rocks (Rosenberg and Stünitz, 2003; Mehl and Hirth, 2008; Boiron et al., 2013; Satsukawa et al., 2013) and in experimentally deformed anorthite aggregates (Ji et al., 2000, 2004). This CPO pattern is commonly attributed to dislocation glide with activation of the dominant (010)[100] slip system or to anisotropic growth at high temperature (Ji et al., 2000, 2004; Satsukawa et al., 2013). Finally, as suggested by quartz CPO, the weakly deformed samples may also register a different strain regime (more coaxial) than moderately and strongly deformed ones. Correlations between the strain regime and the feldspar CPO have already been highlighted by previous studies (Kruhl, 1987; Heidelbach et al., 2000; Ildefonse and Mainprice, 2005; Satsukawa et al., 2013).

5.1.3. Biotite and amphibole

The biotite CPOs (Fig. 6) for amphibolites facies samples GD06-07, GD06-16 and 12-CJB-12D and for granulites facies samples RPM98-122 and RPM98-138, with the [001] axes (or c-axes) oriented perpendicular to the foliation plane, are commonly interpreted as being typical of plastic deformation with basal glide (Barruol and Mainprice, 1993a; Ji et al., 1993; Lloyd et al., 2009; Nishizawa and Kanagawa, 2010; Valcke et al., 2006; and references therein). From TEM analysis of experimentally deformed biotite, Christoffersen and Kronenberg (1993) show that this CPO is related to the activation of (001)[100] and (001)[110] slip systems. Weakly deformed granulite-facies samples (RPM98-166 and RPM98-120) show no clear orientation or relationship with the structural axes (X, Y, Z). However, biotite grains are rare in the later samples, thus the CPO is based on a small number of crystals. Moreover, these biotite grains are crystallized in all directions, mainly around orthopyroxene–quartz–oxide assemblages. Microstructural analysis argues for a secondary crystallization of these biotite grains following the granulite facies deformation stage (Pelletier, 2001) and the lack of clear CPO in these samples reveals the absence of plastic deformation in these minerals. Observation of randomly oriented secondary biotite in less deformed granulite-facies samples allows us to conclude that (1) the retrogression of the granulite facies crust, associated with hydration and late-crystallization of biotite (Opx = > Bt + Qz + Ilm), occurred after the deformation in granulite-facies conditions, and (2) the 1.7 Ga deformation in amphibolite-facies conditions was localized into shear zones and did not affect the granulite-facies cores.

Amphibole fabric measurements in samples from Correll Nunatak suggest dislocation glide with activation of the dominant (100)[001] slip system (Fig. 6). This slip system has already been identified in amphibolite rocks from the intermediate and lower crust (Ji et al., 1993, 2013; Kitamura, 2006; Tatham et al., 2008; McNamara et al., 2012; Getsinger and Hirth, 2014). In sample GD06-16, the secondary (010)[001] slip system could also be activated. Activation of this secondary slip system has already been reported in naturally deformed samples (Imon et al., 2004; Kitamura, 2006; Díaz Aspiroz et al., 2007; Tatham et al., 2008; Llana-Fúnez and Brown, 2012). In their experimental study, Ko and Jung (2015) did not observe the activation of the (010)[001] slip system for temperatures ranging from 0 to 700 °C at 1 GPa, and the presence of this slip system could thus indicate a higher temperature of deformation.

5.1.4. Orthopyroxene

In granulite samples, we identify different orthopyroxene CPO patterns (Fig. 7). The two strongly deformed samples present a similar CPO, whose patterns has already been identified in numerous studies (Barruol and Mainprice, 1993a; Ji et al., 1993; Egydio-Silva et al., 2002; Lund et al., 2006; Kanagawa et al., 2008; Raimbourg et al., 2011 for crustal rock studies). This CPO is usually interpreted as evidence of plastic deformation by dislocation glide with activation of the dominant (100)[001] slip system. We refer to this fabric as the "common" CPO. In the weakly deformed samples (RPM98-118, RPM98-120 and RPM98-166) the fabric is different and less common. These samples show (010) oriented parallel to the foliation plane, [001]-axes parallel to the stretching lineation, and clustering of [100] close to the Y structural direction. We refer to this fabric as the "uncommon" CPO. The moderately deformed sample RPM98-122 presents a composite fabric, combining both "common" and "uncommon" CPOs. Temperature, pressure, chemical composition and water-content are known to influence the deformation processes. Such control by intensive parameters has been well documented for some minerals, as for example olivine (Jung and Karato, 2001; Couvy et al., 2004; Katayama and Karato, 2006). Likewise, we discuss the influence of these factors on CPO development in naturally deformed orthopyroxene from the deep continental crust.

Measurements of activation of secondary (010)[100] slip systems in naturally deformed Mg-rich orthopyroxene were performed by Steuten and Van Roermund (1989) on alpine-type peridotite using TEM observations. More recently, Manthilake et al. (2013) highlighted the effects of aluminium and water-content on activated slip systems in experimentally deformed orthopyroxene. Nazé et al. (1987) and Ross and Nielsen (1978) conducted TEM investigations on natural and experimental orthopyroxenes and experimental deformation on wet polycrystalline enstatite, respectively. They both concluded that activation of (010)[001] needs higher temperature and strain rate conditions than for (100)[001]. These observations are in agreement with those of Ji and Salisbury (1993) and Egydio-Silva et al. (2002) and the observed orthopyroxene CPO could be then developed by the activation of the dominant (100)[001] and secondary (010)[001] slip systems in high-grade amphibolite to granulite-facies samples. "Uncommon" orthopyroxene CPOs were also observed in granulite rocks by Lund et al. (2006). These authors attribute the orthopyroxene CPO variations to the spatial distribution of orthopyroxene grains. The uncommon CPO is observed in the isolated grains in a quartz–feldspathic matrix, which suffered higher differential stresses than clustered grains.

In our samples, the chemical composition of the orthopyroxene does not seem to play a significant role, as the orthopyroxene in all the samples is similar in composition. Thus we cannot directly link Al_2O_3 or Fe0 or Mg0-contents to the variation in orthopyroxene CPO patterns. On the

hand, as observed by Lund et al. (2006) in samples from granulites in the Napier Complex, we measured an "uncommon" CPO in isolated orthopyroxene grains in samples RPM98-118, RPM98-120 and RPM98-166, as opposed to a "common" CPO observed in clustered grains in GD06-28. However, the origin of the "uncommon" fabric development proposed by Lund et al. (2006) is not in agreement with samples RPM98-122 and RPM98-114 where the "common" fabric is found in isolated grains. In our study, the main difference between samples that display "common" and "uncommon" CPOs is their microstructure. Thus, RPM98-166, RPM98-120 and RPM98-118 show evidence of annealing, marked by polycrystalline feldspar mosaics with angles close to 120° and no evidence of intra-grain plastic deformation. Samples RPM98-114 and GD06-28 are mylonitic with a lineation marked by pyroxene alignment and quartz ribbon elongation. Both samples also show clear evidence of dynamic recrystallization, containing orthopyroxene neoblasts, kink bands and subgrains in porphyroclasts. Sample RPM98-122 contains evidence of contrasting deformation intensity, with deformation bands containing quartz with light undulose extinction and static recrystallized bands containing feldspar with characteristic angles of 120°. Therefore, "uncommon" fabrics could be associated with annealing processes, but further studies are needed to test this hypothesis. In particular, water content measurements, experimental deformation and static recrystallization could be useful to gain insight into how the "uncommon" orthopyroxene fabric may develop and under what conditions. Moreover, it could be interesting to carry out a TEM investigation in order to investigate the activation of the (010)[001] slip system during the development of the "uncommon" fabric. We would also like to be clear that this study focuses on crustal deformation whereas the "uncommon" fabric can also affect mantle deformation as it has been observed in peridotite studies (Christensen and Lundquist, 1982; Vauchez and Garrido, 2001; Tommasi et al., 2008; Jung et al., 2010; Baptiste et al., 2012). It is thus very important to improve our understanding of the processes associated with the orthopyroxene CPO variations.

5.2. Deformation in the MSZ

5.2.1. Spatial and temporal variations of the deformation

Macroscopic and microscopic observations of samples allow us to distinguish two stages of deformation. The older one is observed in tectonic boudins preserved during the later tectonic event. This first stage took place under granulite-facies conditions during the Neoarchean regional tectonic and metamorphic event at about 2.5 to 2.4 Ga. This high-temperature deformation led to weakly, moderately and strongly deformed rocks. In the granulite facies samples, both microstructures and CPO analysis argue for a change in deformation mechanisms from weakly deformed rocks with no evidence of plastic deformation or static recrystallization, to strongly deformed rocks (mylonites) forming shear bands from micrometrical to plurimetrical scale which show evidence of plastic deformation. The evolution of active deformation mechanisms is particularly visible in quartz microstructures from moderately to strongly deformed rocks as they present variable microstructures characteristic of subgrain rotation (SGR) and grain boundary migration (GBM) that reflect an increase in diffusion creep processes. In addition, moderately and strongly deformed granulite-facies samples display contrasted quartz CPO suggesting changes in strain regimes. Feldspar in granulite facies samples shows also microstructures with undulose extinction and indented boundaries more common in the most strongly deformed samples. However, there is a phase of major feldspar recrystallization in some samples, which partially erased evidence of plastic deformation. Biotite alignment and the fabric resulting from basal glide is also due to the Neoarchean deformation for moderately to strongly deformed granulite facies samples. On the contrary, weakly deformed rocks (or those with intense annealing) contain randomly oriented post-granulitic biotite crystals. Finally, orthopyroxene is present in granulites facies samples as large rounded grains in weakly deformed sample, and as porphyroclasts and neoblasts in mylonites. These results confirm terrain-scale observations about granulite facies deformation variations as described at Aurora, Stillwell and Cape Gray (see Figs. 2 and 3).

The last stage of deformation is represented by the 1.7 Ga amphibolite-facies samples. It is characterized by a penetrative deformation at Correll Nunatak located in the core of the MSZ, and by narrow shear bands elsewhere in the Neoarchean granulite facies domain. The Palaeoproterozoic deformation is marked by well-defined boundaries between shear bands and cores of preserved rocks that did not undergo the Palaeoproterozoic deformation. This localized deformation appears through many shear zones in the world (Ramsay, 1980; Platt and Behrmann, 1986; Mohanty and Ramsay, 1994; Tommasi et al., 1994, 1995; Neves and Vauchez, 1995; Brown and Solar, 1998; Zhou et al., 2002; Oliot et al., 2014) and could thus be a feature of the intermediate crustal deformation.

5.2.2. Deformation conditions and cinematic

The preserved deformation microstructures in granulite-facies samples from the Neoarchean domain allow us to study the deformation conditions of the 2.4 Ga orogenic event. In particular, a study of the quartz CPO reveals that these recorded deformation events occurred in similar or higher temperature conditions than during the 1.7 Ga event. Pelletier (2001) estimated the pressure–temperature for sample RPM98-114 to be 800 °C, 8.9 kbar and 715 °C, 5 kbar at peak metamorphism and during retrogression, respectively. The symmetric quartz [0001]-axis cross-girdles of the moderately deformed samples indicate a predominantly pure shear deformation. Finally, RPM98-166 and RPM98-120 constitute the less deformed granulites of the TAC. They show evidence of plastic deformation with a high degree of recrystallization in feldspar microstructures. The "uncommon" fabric of the orthopyroxene in these samples could also be related to an intense annealing stage.

Amphibolite facies samples RPM98-106, GD06-07, GD06-08, GD06-10, GD06-12, GD06-16 and GD06-18 (from Correll Nunatak) and 12-CJB-12D (Stillwell Island) are representative of localized shear zones probably related to the 1.7 Ga deformation event (Figs. 2 and 3). They show evidence of strong plastic deformation. Moreover, in the amphibolite rocks from the MSZ, some samples show a clear asymmetry of [11–20] and [0001]-axes. These fabrics argue for a strong simple shear component (Bouchez et al., 1983; Simpson and Schmid, 1983). This result is concordant with microstructural and terrain-scale observations where most textural indicators reveal simple shear activation with a dextral sense (Talarico and Kleinschmidt, 2003; Ménot et al., 2005).

5.3. Crustal seismic anisotropy generated by the MSZ

5.3.1. Seismic model of the deformed lower crust

The seismic anisotropy computation of monomineral aggregates shows that the biotite and amphibole contents are the main contributors to seismic anisotropy, as they represent the two most anisotropic phases of the continental crust. This result is in agreement with many previous studies (Siegesmund et al., 1989; Ji and Salisbury, 1993; Ji et al., 1993, 2015; Barruol and Kern, 1996; Weiss et al., 1999; Godfrey et al., 2000; Tatham et al., 2008; Lloyd et al., 2009; Nishizawa and Kanagawa, 2010; Ward et al., 2012).

The P- and S-wave velocity models created from modal compositions, measured CPO and elastic constants of the different phases allow us to conclude that the deformed crust of the TAC can be considered as being seismically isotropic (less than 1% anisotropy for both amphibolite and granulite facies crustal sections). A similar conclusion was reached by Barruol and Mainprice (1993b); Ji et al. (1993); and Weiss et al. (1999) for mafic rocks and rocks low in amphibole and biotite. Moreover, the studies of Ji et al. (1993) and Ward et al. (2012) show that the assemblage with different phases has a reduced magnitude

of seismic anisotropy, for example interactions between feldspar and quartz or pyroxene, or between micas and quartz respectively. In our case, the crust appears to be isotropic, in particular for S (or SKS) wave propagation, because of the low amphibole and biotite contents observed in the various rock formations of the TAC and because of interactions between the CPO of the different phases. The calculated model is different from those of Almqvist et al. (2013) and Ferré et al. (2014), who also modelled the seismic properties of a crustal shear zone and a late Archean crust, respectively. Differences between the seismic models reflect the mineralogical contrasts between the studied samples and thus highlight the importance of representative samples used to perform lithospheric seismic studies in a specific region.

5.3.2. Contribution to the interpretation of SKS data in the TAC

A seismological study of the Terre Adélie and George V Land region was done by Lamarque et al. (2015), who used SKS anisotropy to interpret mantle structures beneath the TAC and the MSZ. The SKS waves are propagating vertically from the core–mantle boundary to the Earth's surface. Thus, they sample the entire mantle and the crust. If they cross an anisotropic layer, they are split into two perpendicular polarized shear waves propagating at different velocities. In the mantle, because of the CPO pattern of olivine, the orientation of the polarization plane of the fast split shear waves is directly related to the orientation of the foliation and the lineation. Results of Lamarque et al. (2015) show similar orientation of the polarization plane of the fast split shear waves across the TAC. To interpret these results, the authors assumed no crustal contribution and they conclude that the TAC is characterized by constant mantle structures. In this study, we performed a seismic crustal model to evaluate the contribution of the crust to the anisotropy of SKS waves. In the case of the MSZ, which is oriented north–south with a vertical foliation and a sub-horizontal lineation, the SKS waves will cross the crust parallel to Y-axis.

As the crustal section affected by the MSZ displays isotropic seismic features, we propose: (i) that all the anisotropy registered by the SKS-wave study of Lamarque et al. (2015) is due to mantle deformation, and (ii) that the MSZ crustal deformation has no impact on the consistency of the SKS results between stations situated above the craton and above the MSZ (see Fig. 9). These results suggest that the mantle preferred orientation is homogenous throughout the TAC and that the MSZ does not extend into the mantle. However, these new results do not permit us to eliminate the possibility that a former extension of the MSZ into the lithospheric mantle has been erased by a more recent tectonic event as for example, rifting associated with Southern Ocean opening.

6. Conclusions

The study of amphibolite-to-greenschist-facies rocks sampled along the Palaeoproterozoic Mertz shear zone, as well as the tectonic boudins of the Neoarchean granulite-facies domain in the Terre Adélie Craton allow us to look in detail the deformation

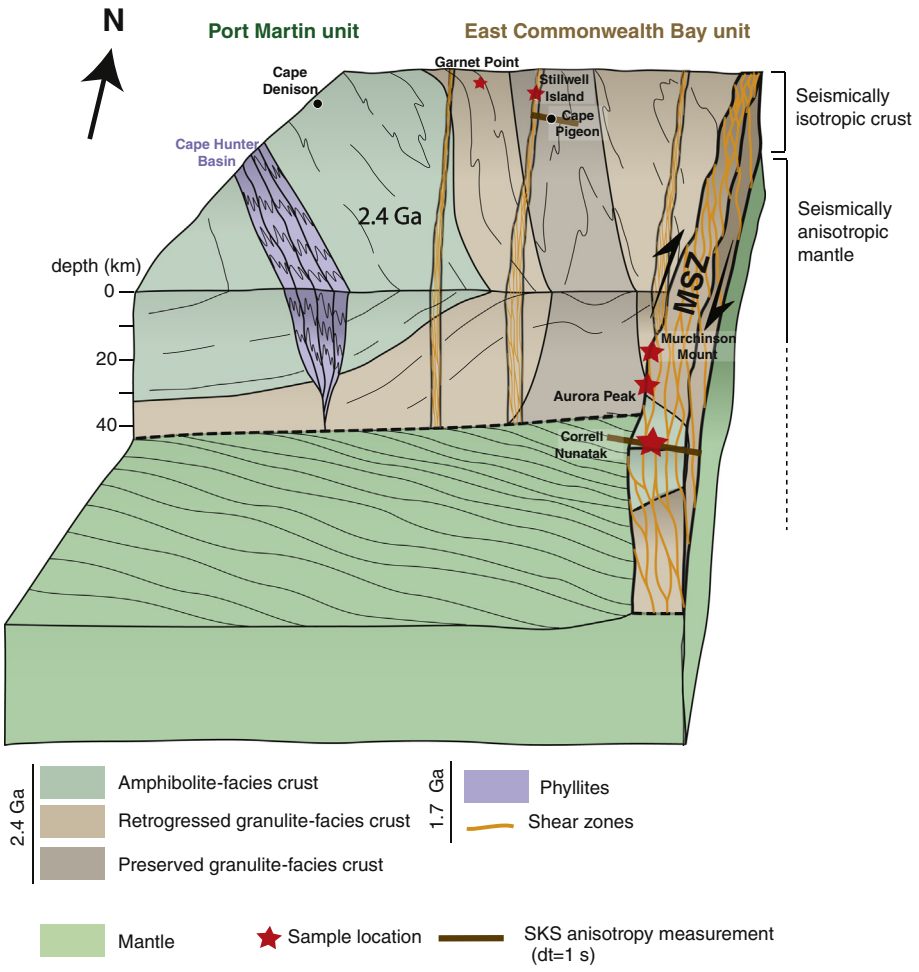

Fig. 9. Synthetic 3D-diagram including observed crustal structures and interpreted mantle structures from the seismological data (SKS anisotropy measurements, Lamarque et al., 2015) and the seismic model of the crust from this study.

processes from a crystal to lithospheric scale. We have found the following:

(1) The Palaeoproterozoic amphibolite-facies deformation is penetrative in the core of the MSZ (at Correll Nunatak). Elsewhere in the TAC, this deformation is more localized, forming narrow shear bands constituted of moderately to strongly deformed rocks. The transition between shear bands and tectonic boudins is sharp. The deformation in the MSZ predominantly occurred under simple shear strain regime.
(2) The Neoarchean granulite-facies deformation is preserved in tectonic boudins (unaffected by the MSZ deformation). This pervasive deformation is characterized by a gradient from weakly to strongly deformed samples, and a retrogression event characterized by marked stages of dynamic and static recrystallization. Pure shear is a strong component of the granulite-facies deformation, especially for moderately deformed samples.
(3) Both events involved plastic deformation processes. Mylonites forming the MSZ recorded dominant SGR with subordinate GBM processes at medium temperatures during simple shear. The granulite-facies boudins record predominant GBM with subordinate SGR at higher temperatures, followed by predominant SGR processes during retrogressive recrystallization.
(4) These processes led to the development of various CPO patterns of minerals:
   – Quartz CPOs related to the MSZ rocks are characterized by a single asymmetric girdle of [0001]-axes interpreted as resulting of the prismatic <a> and rhomboidal <a> slip systems activation in mylonite samples and prismatic <a>, rhomboidal <a> and basal <a> slip systems activation in moderately deformed rocks. In the granulite rocks, mylonites are characterized by the activation of a prismatic <a> (and rhomboidal <a> for some samples) slip systems with subsidiary activation of basal <a> slip, probably related to retrogression. Moderately deformed samples have quartz CPO with a symmetric cross girdle form indicating activation of prismatic <a>, rhomboidal <a> and basal <a> slip systems.
   – Maxima densities of feldspar CPO are weak. This lack of strong crystallographic fabrics can be interpreted in terms of high temperature deformation. The clearest fabrics were observed in granulite-facies samples with evidence of a marked static recrystallization stage.
   – Biotites show a well-marked CPO related to basal glide except for biotites that recrystallized during the retrogression of weakly deformed granulite-facies samples.
   – Amphibole fabric measurements in samples from the MSZ suggest dislocation glide with activation of the dominant (100)[001] slip system.
   – Orthopyroxene CPOs are characterized by a “common” fabric related to the activation of the (100)[001] slip system in strongly deformed samples. In weakly deformed samples, affected by annealing processes, we observed an “uncommon” fabric characterized by (010) oriented parallel to the foliation plane and [001]-axes parallel to the lineation. Moderately deformed samples display a “composite” fabric that combines patterns from the “common” and “uncommon” fabrics.
(5) Based on the seismic property model, we highlight that the crust affected by the MSZ could be isotropic, in particular for the teleseismic S (or SKS) wave propagation. Consequently, all the seismic properties registered by the SKS-wave study of Lamarque et al. (2015) in various sites of the TAC are due to mantle deformation. There is no evidence of the MSZ extending downwards into the mantle. This could be due to a homogeneous structuration of the mantle beneath the entire TAC.

Acknowledgements

This work was supported by the French Polar Institute (IPEV, Institut Paul Emile Victor) through the programme ArLiTA (Architecture de la Lithosphère de Terre Adélie). ArLiTA also benefited of the support of the INSU-SYSTER programme. We also want to thank Fabrice Barou (Université de Montpellier), Sergio Sao-Joao and Marilyne Mondon (Ecole des Mines de Saint-Etienne) for efficient support during EBSD acquisition. Thanks are due to Colette Alboussière and Chantal Perrache (Université Jean Monnet, Saint-Etienne) for the excellent quality of the analysed thin sections. We thank also Andréa Tommasi, Fatna Kourime and Giulia Palazzin for discussions about CPO studied minerals. The constructive review by Shaocheng Ji was highly appreciated.

Supplementary data

Supplementary data to this article can be found online at http://dx.doi.org/10.1016/j.tecto.2016.05.011.

References

Adissin Glodji, L., Bascou, J., Yessoufou, S., Ménot, R.P., Villaros, A., 2014. Relationships between deformation and magmatism in the Pan-African Kandi Shear Zone: Microstructural and AMS studies of Ediacaran granitoid intrusions in central Bénin (West Africa). J. Afr. Earth Sci. 97, 143–160. http://dx.doi.org/10.1016/j.jafrearsci.2014.04.012.

Aleksandrov, K.S., Ryzhova, T.V., 1961. The elastic properties of rock forming minerals II: Layered silicates. Izv. Acad. Sci. USSR, Geophys. Phys. Solid Earth 1165–1168.

Aleksandrov, K.S., Alchikov, U.V., Belikov, B.P., Zaslavskii, B.I., Krupnyi, A.I., 1974. Velocities of elastic waves in minerals at atmospheric pressure and increasing precision of elastic constants by means of EVM (in Russian). Izv. Acad. Sci. USSR, Geol. Ser. 10, 15–24.

Almqvist, B.S.G., Hirt, A.M., Herwegh, M., Ebert, A., Walter, J.M., Leiss, B., Burlini, L., 2013. Seismic anisotropy in the Morcles nappe shear zone: Implications for seismic imaging of crustal scale shear zones. Tectonophysics 603, 162–178. http://dx.doi.org/10.1016/j.tecto.2013.05.025.

Alsop, G.I., Holdsworth, R.E., 2004. Shear zones — an introduction and overview. Geol. Soc. Lond., Spec. Publ. 224, 1–9.

Anderson, J.L., Cullers, R.L., 1999. Paleo- and Mesoproterozoic granite plutonism of Colorado and Wyoming. Rocky Mt. Geol. 34 (2), 149–164.

Augenstein, C., Burg, J.P., 2011. Natural annealing of dynamically recrystallised quartzite fabrics: Example from the Cévennes, SE French Massif Central. J. Struct. Geol. 33 (3), 244–254. http://dx.doi.org/10.1016/j.jsg.2010.10.008.

Babuska, V., Fiala, J., Kumazawa, M., Ohno, I., Sumino, Y., 1978. Elastic properties of garnet solid-solution series. Phys. Earth Planet. Inter. 16, 157–176.

Baptiste, V., Tommasi, A., Demouchy, S., 2012. Deformation and hydration of the lithospheric mantle beneath the Kaapvaal craton. South Africa, Lithos 149, 31–50. http://dx.doi.org/10.1016/j.lithos.2012.05.001.

Barker, S.L., Sibson, R.H., Palin, J.M., FitzGerald, J.D., Reddy, S., Warr, L.N., van der Pluijm, B.a., 2010. Cretaceous age, composition, and microstructure of pseudotachylyte in the Otago Schist, New Zealand, New Zeal. J. Geol. Geophys. 53, 15–29. http://dx.doi.org/10.1080/00288301003631764.

Barruol, G., Kern, H., 1996. Seismic anisotropy and shear-wave splitting in lower-crustal and upper-mantle rocks from the Ivrea Zone—experimental and calculated data. Phys. Earth Planet. Inter. 95 (3–4), 175–194. http://dx.doi.org/10.1016/0031-9201(95)03124-3.

Barruol, G., Mainprice, D., 1993a. 3D seismic velocities calculated from lattice-preferred orientation and reflectivity of lower crustal section: examples of the Val Sesia section (Ivrea zone, northern Italy). Geophys. J. Int. 115, 1169–1188.

Barruol, G., Mainprice, D., 1993b. A quantitative evaluation of the contribution of crustal rocks to the shear-wave splitting of teleseismic SKS waves. Phys. Earth Planet. Inter. 78, 281–300.

Bass, J.D., Weidner, D.J., 1984. Elasticity of single crystal of orthoferrosilite. J. Geophys. Res. 89, 4359–4371.

Benn, K., Allard, B., 1989. Preferred mineral orientations related to magmatic flow in ophiolite layered gabbros. J. Petrol. 30 (1988), 925–946.

Boiron, T., Bascou, J., Camps, P., Ferre, E.C., Maurice, C., Guy, B., Gerbe, M.-C., Launeau, P., 2013. Internal structure of basalt flows: insights from magnetic and crystallographic fabrics of the La Palisse volcanics, French Massif Central. Geophys. J. Int. 193 (2), 585–602. http://dx.doi.org/10.1093/gji/ggs115.

Borradaile, G.J., Henry, B., 1997. Tectonic applications of magnetic susceptibility and its anisotropy. Earth-Sci. Rev. 42, 49–93. http://dx.doi.org/10.1016/S0012-8252(96)00044-X.

Bouchez, J.L., Nicolas, A., Lister, G., 1983. Fabric asymmetry and shear sense in movement zones. Geol. Rundsch. 72, 401–419.

Boullier, A.-M., Bertrand, J.-M., 1981. Tectonique tangentielle profonde et couloirs mylonitiques dans le Hoggar central polycyclique (Algérie). Bull. Soc. Geol. Fr. XXXII (1), 17–22 (7 t.).

Brown, M., Solar, G.S., 1998. Shear-zone systems and melts: feedback relations and self-organization in orogenic belts. J. Struct. Geol. 20 (213), 211–227. http://dx.doi.org/10.1016/S0191-8141(97)00068-0.

Bunge, 1982. Texture Analysis in Materials Sciences. Buttlewort, London.
Burov, E.B., 2011. Rheology and strength of the lithosphere. Mar. Pet. Geol. 28 (8), 1402–1443. http://dx.doi.org/10.1016/j.marpetgeo.2011.05.008.
Chernak, L.J., Hirth, G., Selverstone, J., Tullis, J., 2009. Effect of aqueous and carbonic fluids on the dislocation creep strength of quartz. J. Geophys. Res. 114, B04201. http://dx.doi.org/10.29/2008JB005884.
Christensen, N.I., Lundquist, S.M., 1982. Pyroxene orientation within the upper mantle. Geol. Soc. Am. Bull. 93 (4), 279–288. http://dx.doi.org/10.1130/0016-7606(1982)93<279:POWTUM>2.0.CO;2.
Christoffersen, R., Kronenberg, A.K., 1993. Dislocation interactions in experimentally deformed biotite. J. Struct. Geol. 15 (9), 1077–1095.
Collins, M.D., Brown, J.M., 1998. Elasticity of an upper mantle clinopyroxene. Phys. Chem. Miner. 26, 7–13.
Couvy, H., Frost, D.J., Heidelbach, F., Nyilas, K., Ungár, T., Mackwell, S., Cordier, P., 2004. Shear deformation experiments of forsterite at 11 GPa–1400 °C in the multianvil apparatus. Eur. J. Mineral. 16 (6), 877–889. http://dx.doi.org/10.1127/0935-1221/2004/0016-0877.
Dhuime, B., C. J. Hawkesworth, P. A. Cawood, and C. D. Storey (2012), A change in the geodynamics of continental growth 3 billion years ago, Science (80-.)., 335, 1334–1337.
Di Vincenzo, G., Talarico, F., Kleinschmidt, G., 2007. An $^{40}Ar/^{39}Ar$ investigation of the Mertz Glacier area (George V Land, Antarctica): implications for the Ross Orogen–East Antarctic Craton relationship and Gondwana reconstructions. Precambrian Res. 152 (3–4), 93–118. http://dx.doi.org/10.1016/j.precamres.2006.10.002.
Díaz Aspiroz, M., Lloyd, G.E., Fernández, C., 2007. Development of lattice preferred orientation in clinoamphiboles deformed under low-pressure metamorphic conditions. A SEM/EBSD study of metabasites from the Aracena metamorphic belt (SW Spain). J. Struct. Geol. 29 (4), 629–645. http://dx.doi.org/10.1016/j.jsg.2006.10.010.
Duclaux, G., Rolland, Y., Ruffet, G., Ménot, R.-P., Guillot, S., Peucat, J.-J., Fanning, M., Rey, P., Pêcher, A., 2008. Superimposed Neoarchaean and Paleoproterozoic tectonics in the Terre Adélie Craton (East Antarctica): Evidence from Th–U–Pb ages on monazite and $^{40}Ar/^{39}Ar$ ages. Precambrian Res. 167 (3–4), 316–338. http://dx.doi.org/10.1016/j.precamres.2008.09.009.
Egydio-Silva, M., Vauchez, A., Bascou, J., Hippertt, J., 2002. High-temperature deformation in the Neoproterozoic transpressional Ribeira belt, southeast Brazil. Tectonophysics 352 (1–2), 203–224. http://dx.doi.org/10.1016/S0040-1951(02)00197-X.
Egydio-Silva, M., Vauchez, A., Raposo, M.I.B., Bascou, J., Uhlein, A., 2005. Deformation regime variations in an arcuate transpressional orogen (Ribeira belt, SE Brazil) imaged by anisotropy of magnetic susceptibility in granulites. J. Struct. Geol. 27 (10), 1750–1764. http://dx.doi.org/10.1016/j.jsg.2005.06.001.
Etchecopar, A., 1977. A plane kinematic model of progressive deformation in a polycrystalline aggregate. Tectonophysics 39, 121–139.
Fanning, C., Ménot, R.P., Peucat, J., Pelletier, A., 2002. A closer examination of the direct links between Southern Australia and Terre Adélie and George V Land, Antarctica, in 16th Australian Geological Convention. Adelaide.
Ferré, E.C., Gébelin, A., Conder, J.A., Christensen, N., Wood, J.D., Teyssier, C., 2014. Seismic anisotropy of the Archean crust in the Minnesota River Valley, Superior Province. Geophys. Res. Lett. 1–9. http://dx.doi.org/10.1002/2013GL059116.
Gandais, M., Willaime, C., 1984. Mechanical properties of feldspars. In: Brown, W.L. (Ed.), Feldspars and Feldspathoids, pp. 207–246 (Dordrecht).
Gapais, D., Pelletier, A., Ménot, R.-P., Peucat, J.-J., 2008. Paleoproterozoic tectonics in the Terre Adélie Craton (East Antarctica). Precambrian Res. 162 (3–4), 531–539. http://dx.doi.org/10.1016/j.precamres.2007.10.011.
Getsinger, A.J., Hirth, G., 2014. Amphibole fabric formation during diffusion creep and the rheology of shear zones. Geology 42 (6), 535–538. http://dx.doi.org/10.1130/G35327.1.
Gibson, G.M., Totterdell, J.M., White, L.T., Mitchell, C.H., Stacey, A.R., Morse, M.P., Whitaker, A., 2013. Pre-existing basement structure and its influence on continental rifting and fracture zone development along Australia's southern rifted margin. J. Geol. Soc. Lond. 170 (2), 365–377. http://dx.doi.org/10.1144/jgs2012-040.
Godfrey, N.J., Christensen, N.I., Okaya, D.A., 2000. Anisotropy of schists: Contribution of crustal anisotropy to active source seismic experiments and shear wave splitting observations. J. Geophys. Res. 105 (B12), 27991. http://dx.doi.org/10.1029/2000JB900286.
Grujic, D., Mancktelow, N.S., 1998. Melt-bearing shear zones: analogue experiments and comparison with examples from southern Madagascar. J. Struct. Geol. 20 (6), 673–680.
Hamilton, W.B., 1998. Archean magmatism and deformation were not products of plate tectonics. Precambrian Res. 91, 143–179.
Haussühl, E., Vinograd, V.L., Krenzel, T.F., Schreuer, J., Wilson, D.J., Ottinger, J., 2011. High temperature elastic properties of Mg-cordierite: experimental studies and atomistic simulations. Z. Krist. 226 (3), 236–253. http://dx.doi.org/10.1524/zkri.2011.1307.
Heidelbach, F., Post, A., Tullis, J., 2000. Crystallographic preferred orientation in albite samples deformed experimentally by dislocation and solution precipitation creep. J. Struct. Geol. 22, 1649–1661.
Holyoke, C.W., Kronenberg, A.K., 2013. Reversible water weakening of quartz, Earth Planet. Sci. Lett. 374, 185–190.
Ildefonse, B., Mainprice, D., 2005. Modeling the viscous to plastic transition in mid-ocean ridge gabbros: implications for crystallographic preferred orientation of plagioclase and seismic anisotropy. AGU Fall Meeting (p. #MR33A–0159).
Imon, R., Okudaira, T., Kanagawa, K., 2004. Development of shape- and lattice-preferred orientations of amphibole grains during initial cataclastic deformation and subsequent deformation by dissolution-precipitation creep in amphibolites from the Ryoke metamorphic belt, SW Japan. J. Struct. Geol. 26 (5), 793–805. http://dx.doi.org/10.1016/j.jsg.2003.09.004.
Jessell, M.W., Lister, G.S., 1990. A simulation of the temperature dependence of quartz fabrics. Geol. Soc. Lond., Spec. Publ. 54, 353–362. http://dx.doi.org/10.1144/GSL.SP.1990.054.01.31.
Ji, S., Salisbury, M.H., 1993. Shear-wave velocities, anisotropy and splitting in high-grade mylonites. Tectonophysics 221 (3–4), 453–473. http://dx.doi.org/10.1016/0040-1951(93)90173-H.
Ji, S., Salisbury, M.H., Hanmer, S., 1993. Petrofabric, P-wave anisotropy and seismic reflectivity of high-grade tectonites. Tectonophysics 222, 195–226.
Ji, S., Wirth, R., Rybacki, E., Jiang, Z., 2000. High-temperature plastic deformation of quartz–plagioclase multilayers by layer-normal compression. J. Geophys. Res. 105 (B7), 16651. http://dx.doi.org/10.1029/2000JB900130.
Ji, S., Jiang, Z., Rybacki, E., Wirth, R., Prior, D., Xia, B., 2004. Strain softening and microstructural evolution of anorthite aggregates and quartz–anorthite layered composites deformed in torsion. Earth Planet. Sci. Lett. 222 (2), 377–390. http://dx.doi.org/10.1016/j.epsl.2004.03.021.
Ji, S., Shao, T., Michibayashi, K., Long, C., Wang, Q., Kondo, Y., Zhao, W., Wang, H., Salisbury, M.H., 2013. A new calibration of seismic velocities, anisotropy, fabrics, and elastic moduli of amphibole-rich rocks. J. Geophys. Res. Solid Earth 118 (9), 4699–4728. http://dx.doi.org/10.1002/jgrb.50352.
Ji, S., Shao, T., Salisbury, M.H., Sun, S., Michibayashi, K., Zhao, W., Long, C., Liang, F., Satsukawa, T., 2014. Plagioclase preferred orientation and induced seismic anisotropy in mafic igneous rocks. J. Geophys. Res. Solid Earth 119, 1–25. http://dx.doi.org/10.1002/2014JB011352.Received.
Ji, S., Shao, T., Michibayashi, K., Oya, S., Satsukawa, T., Wang, Q., Zhao, W., Salisbury, M.H., 2015. Magnitude and symmetry of seismic anisotropy in mica- and amphibole-bearing metamorphic rocks and implications for tectonic interpretation of seismic data from southeast Tibetan Plateau. J. Geophys. Res. Solid Earth 120. http://dx.doi.org/10.1002/2015JB012218.Received.
Jiang, Z., Prior, D.J., Wheeler, J., 2000. Albite crystallographic preferred orientation and grain misorientation distribution in a low-grade mylonite: implications for granular flow. J. Struct. Geol. 22, 1663–1674.
Jordan, T.A., Ferraccioli, F., Armadillo, E., Bozzo, E., 2013. Crustal architecture of the Wilkes Subglacial Basin in East Antarctica, as revealed from airborne gravity data. Tectonophysics 585, 196–206. http://dx.doi.org/10.1016/j.tecto.2012.06.041.
Jung, H., Karato, S., 2001. Water-induced fabric transitions in olivine. Science 293 (5534), 1460–1463. http://dx.doi.org/10.1126/science.1062235.
Jung, H., Park, M., Jung, S., Lee, J., 2010. Lattice preferred orientation, water content, and seismic anisotropy of orthopyroxene. J. Earth Sci. 21 (5), 555–568. http://dx.doi.org/10.1007/s12583-010-0118-9.
Kanagawa, K., Shimano, H., Hiroi, Y., 2008. Mylonitic deformation of gabbro in the lower crust: A case study from the Pankenushi gabbro in the Hidaka metamorphic belt of central Hokkaido, Japan. J. Struct. Geol. 30 (9), 1150–1166. http://dx.doi.org/10.1016/j.jsg.2008.05.007.
Katayama, I., Karato, S., 2006. Effect of temperature on the B- to C-type olivine fabric transition and implication for flow pattern in subduction zones. Phys. Earth Planet. Inter. 157 (1–2), 33–45. http://dx.doi.org/10.1016/j.pepi.2006.03.005.
Kisters, A.F.M., Gibson, R.L., Charlesworth, E.G., Anhaeusser, C.R., 1998. The role of strain localization in the segregation and ascent of anatectic melts, Namaqualand, South Africa. J. Struct. Geol. 20 (213), 229–242. http://dx.doi.org/10.1016/S0191-8141(97)00081-3.
Kitamura, K., 2006. Constraint of lattice-preferred orientation (LPO) on Vp anisotropy of amphibole-rich rocks. Geophys. J. Int. 165, 1058–1065. http://dx.doi.org/10.1111/j.1365-246X.2006.02961.x.
Kleinschmidt, G., Talarico, F., 2000. The Mertz Shear Zone, Terra Antarct. Report 5, 109–115.
Ko, B., Jung, H., 2015. Crystal preferred orientation of an amphibole experimentally deformed by simple shear. Nat. Commun. 6, 6586. http://dx.doi.org/10.1038/ncomms7586.
Kronenberg, A.K., Tullis, J., 1984. Flow strengths of quartz aggregates: grain size and pressure effects due to hydrolytic weakening. J. Geophys. Res. Solid Earth 89 (B6), 4281–4297.
Kruhl, J.H., 1987. Preferred lattice orientations of plagioclase from amphibolite and greenschist facies rocks near the Insubric Line (Western Alps). Tectonophysics 135, 233–242.
Lamarque, G., Barruol, G., Fontaine, F.R., Bascou, J., Ménot, R.-P., 2015. Crustal and mantle structure beneath the Terre Adelie Craton, East Antarctica: insights from receiver function and seismic anisotropy measurements. Geophys. J. Int. 200 (2), 809–823. http://dx.doi.org/10.1093/gji/ggu430.
Lapworth, T., Wheeler, J., Prior, D.J., 2002. The deformation of plagioclase investigated using electron backscatter diffraction crystallographic preferred orientation data. J. Struct. Geol. 24, 387–399.
Law, R.D., 1990. Crystallographic fabrics: a selective review of their applications to research in structural geology. Geol. Soc. Lond., Spec. Publ. 54 (1), 335–352. http://dx.doi.org/10.1144/GSL.SP.1990.054.01.30.
Law, R.D., 2014. Deformation thermometry based on quartz c-axis fabrics and recrystallization microstructures: A review. J. Struct. Geol. 66, 129–161. http://dx.doi.org/10.1016/j.jsg.2014.05.023.
Lee, C.A., Luffi, P., Höink, T., Li, Z.A., Lenardic, A., 2008. The role of serpentine in preferential craton formation in the late Archean by lithosphere underthrusting. Earth Planet. Sci. Lett. 269, 96–104. http://dx.doi.org/10.1016/j.epsl.2008.02.010.
Li, Z., Chan, S., Garner, F.A., Bradt, R.C., 1995. Elastic stability of high dose neutron irradiated spinel. J. Nucl. Mater. 219, 139–142.
Llana-Fúnez, S., Brown, D., 2012. Contribution of crystallographic preferred orientation to seismic anisotropy across a surface analog of the continental Moho at Cabo Ortegal, Spain. Bull. Geol. Soc. Am. 124 (9–10), 1495–1513. http://dx.doi.org/10.1130/B30568.1.
Lloyd, G., Butler, R., Casey, M., Mainprice, D., 2009. Mica, deformation fabrics and the seismic properties of the continental crust. Earth Planet. Sci. Lett. 288, 320–328. http://dx.doi.org/10.1016/j.epsl.2009.09.035.

Lund, M.D., Piazolo, S., Harley, S.L., 2006. Ultrahigh temperature deformation microstructures in felsic granulites of the Napier Complex, Antarctica. Tectonophysics 427 (1–4), 133–151. http://dx.doi.org/10.1016/j.tecto.2006.05.022.
Mainprice, D., 1990. A fortran program to calculate seismic anisotropy from the lattice preferred orientation of minerals. Comput. Geosci. 16 (3), 385–393.
Mainprice, D.H., Paterson, M.S., 1984. Experimental studies of the role of water in the plasticity of quartzites. J. Geophys. Res. Solid Earth 89 (B6), 4257–4269.
Mancktelow, N.S., Pennacchioni, G., 2004. The influence of grain boundary fluids on the microstructures of quartz-feldspar mylonites. J. Struct. Geol. 26, 47–69.
Manthilake, M.A.G.M., Miyajima, N., Heidelbach, F., Soustelle, V., Frost, D.J., 2013. The effect of aluminum and water on the development of deformation fabrics of orthopyroxene. Contrib. Mineral. Petrol. 165 (3), 495–505. http://dx.doi.org/10.1007/s00410-012-0819-4.
Martelat, J.-E., Schulmann, K., Lardeaux, J., Nicollet, C., Cardon, H., 1999. Granulite microfabrics and deformation mechanisms in southern Madagascar. J. Struct. Geol. 21, 671–687.
McNamara, D.D., Wheeler, J., Pearce, M., Prior, D.J., 2012. Fabrics produced mimetically during static metamorphism in retrogressed eclogites from the Zermatt–Saas zone, Western Italian Alps. J. Struct. Geol. 44, 167–178. http://dx.doi.org/10.1016/j.jsg.2012.08.006.
McSkimin, H.J., Anreatch, J.R., Thruston, R.N., 1965. Elastic moduli of quartz versus hydrostatic pressure at 25 °C and −195.8 °C. J. Appl. Phys. 36, 1624–1632.
Mehl, L., Hirth, G., 2008. Plagioclase preferred orientation in layered mylonites: Evaluation of flow laws for the lower crust. J. Geophys. Res. 113 (B5), B05202. http://dx.doi.org/10.1029/2007JB005075.
Menegon, L., Pennacchioni, G., Heilbronner, R., Pittarello, L., 2008. Evolution of quartz microstructure and c-axis crystallographic preferred orientation within ductilely deformed granitoids (Arolla unit, Western Alps). J. Struct. Geol. 30 (11), 1332–1347. http://dx.doi.org/10.1016/j.jsg.2008.07.007.
Ménot, R., Pêcher, A., Rolland, Y., Peucat, J., Pelletier, A., Duclaux, G., Guillot, S., 2005. Structural setting of the Neoarchean terrains in the Commonwealth Bay Area (143–145°E), Terre Adélie Craton, East Antarctica. Gondwana Res. 8 (1), 1–9.
Ménot, R.P., Duclaux, G., Peucat, J.J., Rolland, Y., Guillot, S., Fanning, M., Bascou, J., Gapais, D., Pêcher, A., 2007. Geology of the Terre Adélie Craton (135–146°E), East Antarctica, in Antarctica: a keystone in a changing world — Online Proceedings for the Tenth International Symposium on Antarctica Earth Sciences. In: Cooper, A., Raymond, C., Al., E. (Eds.), USGS Open-file Report 2007–1047, Extended Abstract, p. 1047.
Mohanty, S., Ramsay, J.G., 1994. Strain partitioning in ductile shear zones: an example from a Lower Pennine nappe of Switzerland. J. Struct. Geol. 16 (5), 663–676.
Nakashima, S., Matayoshi, H., Yuko, T., Michibayashi, K., Masuda, T., Kuroki, N., Yamagishi, H., Ito, Y., Nakamura, A., 1995. Infrared microspectroscopy analysis of water distribution in deformed and metamorphosed rocks. Tectonophysics 245, 263–276.
Nazé, L., Doukhan, N., Doukhan, J.-C., Latrous, K., 1987. A TEM study of lattice defects in naturally and experimentally deformed orthopyroxenes. Bull. Mineral. 110, 497–512.
Neves, S.P., Vauchez, A., 1995. Magma emplacement and shear zone nucleation and development in northeast Brazil (Fazenda Nova and Pernambuco shear zones; State of Pernambuco). J. S. Am. Earth Sci. 8, 289–298. http://dx.doi.org/10.1016/0895-9811(95)00014-7.
Neves, S.P., Vauchez, A., Archanjo, C.J., 1996. Shear zone-controlled magma emplacement or magma-assisted nucleation of shear zones? Insights from northeast Brazil. Tectonophysics 262, 349–364. http://dx.doi.org/10.1016/0040-1951(96)00007-8.
Neves, S.P., Vauchez, A., Feraud, G., 2000. Tectono-thermal evolution, magma emplacement, and shear zone development in the Caruaru area (Borborema Province, NE Brazil). Precambrian Res. 99, 1–32. http://dx.doi.org/10.1016/S0301-9268(99)00026-1.
Nicolas, A., Poirier, J.P., 1976. Crystalline Plasticity and Solid State Flow in Metamorphic Rocks. Wiley, New-York.
Nishizawa, O., Kanagawa, K., 2010. Seismic velocity anisotropy of phyllosilicate-rich rocks: characteristics inferred from experimental and crack-model studies of biotites rich schist. Geophys. J. Int. 182, 375–388. http://dx.doi.org/10.1111/j.1365-246X.2010.04614.x.
Oliot, E., Goncalves, P., Schulmann, K., Marquer, D., Lexa, O., 2014. Mid-crustal shear zone formation in granitic rocks: Constraints from quantitative textural and crystallographic preferred orientations analyses. Tectonophysics 612-613, 63–80. http://dx.doi.org/10.1016/j.tecto.2013.11.032.
Oliver, R., Fanning, C., 2002. Proterozoic geology east and southeast of Commonwealth Bay, George V Land, Antarctica, and its relationship to that of adjacent Gondwana terranes, in Antarctica at the close of the millenium. R. Soc. N. Z., Bull. 35, 51–58.
Passchier, C.W., Trouw, R.A.J., 1996. Microtectonics. Springer-V, Heidelberg.
Pelletier, A., 2001. Etude structurale et métamorphique du socle de Terre Adélie - George V Land (Est Antarctique): un exemple de la transition archéen/paléoprotérozoïque (Unpublished PhD thesis) Université Jean Monnet, Saint Etienne (195pp.).
Pelletier, A., Gapais, D., Ménot, R., Peucat, J., 2002. Tectonique transpressive en terre Adélie au Paléoprotérozoïque (Est Antarctique). C. R. Acad. Sci. Paris 334, 505–511.
Pennacchioni, G., Menegon, L., Leiss, B., Nestola, F., Bromiley, G., 2010. Development of crystallographic preferred orientation and microstructure during plastic deformation of natural coarse-grained quartz veins. J. Geophys. Res. 115 (B12), B12405. http://dx.doi.org/10.1029/2010JB007674.
Peternell, M., Hasalová, P., Wilson, C.J.L., Piazolo, S., Schulmann, K., 2010. Evaluating quartz crystallographic preferred orientations and the role of deformation partitioning using EBSD and fabric analyser techniques. J. Struct. Geol. 32 (6), 803–817. http://dx.doi.org/10.1016/j.jsg.2010.05.007.
Platt, J.P., Behrmann, J.H., 1986. Structures and fabrics in a crustal-scale shear zone, Betic Cordillera, SE Spain. J. Struct. Geol. 8 (1), 15–33. http://dx.doi.org/10.1016/0191-8141(86)90014-3.
Post, A.D., Tullis, J., Yund, R.A., 1996. Effects of chemical environment on dislocation creep of quartzite. J. Geophys. Res. Solid Earth 101 (B10), 22143–22155.
Raimbourg, H., Toyoshima, T., Harima, Y., Kimura, G., 2008. Grain-size reduction mechanisms and rheological consequences in high-temperature gabbro mylonites of Hidaka, Japan. Earth Planet. Sci. Lett. 267 (3–4), 637–653. http://dx.doi.org/10.1016/j.epsl.2007.12.012.
Raimbourg, H., Kogure, T., Toyoshima, T., 2011. Crystal bending, subgrain boundary development, and recrystallization in orthopyroxene during granulite-facies deformation. Contrib. Mineral. Petrol. 162 (5), 1093–1111. http://dx.doi.org/10.1007/s00410-011-0642-3.
Ramsay, J.G., 1980. Shear zone geometry: a review. J. Struct. Geol. 2 (1/2), 83–99.
Rosenberg, C.L., Stünitz, H., 2003. Deformation and recrystallization of plagioclase along a temperature gradient: an example from the Bergell tonalite. J. Struct. Geol. 25, 389–408.
Ross, J.V., Nielsen, K.C., 1978. High-temperature flow of wet polycrystalline enstatite. Tectonophysics 44, 233–261.
Satsukawa, T., Ildefonse, B., Mainprice, D., Morales, L.F.G., Michibayashi, K., Barou, F., 2013. A database of plagioclase crystal preferred orientations (CPO) and microstructures — implications for CPO origin, strength, symmetry and seismic anisotropy in gabbroic rocks. Solid Earth 4, 511–542. http://dx.doi.org/10.5194/se-4-511-2013.
Schmid, S.M., Casey, M., 1986. Complete fabric analysis of some commonly observed quartz c-axis patterns. Geophys. Monogr. 36, 263–286.
Shaw, C.A., Karlstrom, K.E., Williams, M.L., Jercinovic, M.J., Mccoy, A.M., 2001. Electron-microprobe monazite dating of ca. 1.71–1.63 and ca. 1.45–1.38 Ga deformation in the Homestake shear zone , Colorado: Origin and early evolution of a persistent intracontinental tectonic zone. Geology http://dx.doi.org/10.1130/0091-7613(2001)029<0739.
Siegesmund, S., Takeshita, T., Kern, H., 1989. Anisotropy of Vp and Vs in an amphibolite of the deeper crust and its relationship to the mineralogical, microstructural and textural characteristics of the rock. Tectonophysics 157, 25–38.
Silver, P.G., 1996. Seismic anisotropy beneath the continents: Probing the Depths of Geology. Annu. Rev. Earth Planet. Sci. 24, 385–432.
Simpson, C., Schmid, S.M., 1983. An evaluation of criteria to deduce the sense of movement in sheared rocks. Geol. Soc. Am. Bull. 94, 1281–1288.
Steuten, J.M., Van Roermund, H.L.M., 1989. An optical and electron microscopy study of defect structures in naturally deformed orthopyroxene. Tectonophysics 157, 331–338. http://dx.doi.org/10.1016/0040-1951(89)90148-0.
Stillwell, F.L., 1918. The metamorphic rocks of Adélie Land, in Australian Antarctic Expedition 1911–14. Sci. Rep., Ser A. III-Geol.
Stipp, M., Stünitz, H., Heilbronner, R., Schmid, S.M., 2002a. Dynamic recrystallization of quartz: correlation between natural and experimental conditions. Geol. Soc. Lond., Spec. Publ. 15 (c), 171–190.
Stipp, M., Stünitz, H., Heilbronner, R., Schmid, S.M., 2002b. The eastern Tonale fault zone: a "natural laboratory" for crystal plastic deformation of quartz over a temperature range from 250 to 700 °C. J. Struct. Geol. 24, 1861–1884.
Svahnberg, H., Piazolo, S., 2010. The initiation of strain localisation in plagioclase-rich rocks: Insights from detailed microstructural analyses. J. Struct. Geol. 32, 1404–1416.
Talarico, F., Kleinschmidt, G., 2003. Structural an metamorphic evolution of the Mertz Shear Zone (East Antarctic Craton, Geroge V Land): implications for Australia/Antarctica correlations and East Antarctic craton/Ross orogen relationships. Terra Antarct. 10, 229–248.
Tatham, D.J., Lloyd, G.E., Butler, R.W.H., Casey, M., 2008. Amphibole and lower crustal seismic properties. Earth Planet. Sci. Lett. 267 (1–2), 118–128. http://dx.doi.org/10.1016/j.epsl.2007.11.042.
Tommasi, A., Vauchez, A., Fernandes, L.A.D., Porcher, C.C., 1994. Magma-assisted strain localization in an orogen-parallel transcurrent shear zone of southern Brazil. Tectonics 13 (2), 421–437.
Tommasi, A., Vauchez, A., Daudré, B., 1995. Initiation and propagation of shear zones in a heterogeneous continental lithosphere. J. Geophys. Res. 100 (B11), 22083–22101.
Tommasi, A., Vauchez, A., Ionov, D.A., 2008. Deformation, static recrystallization, and reactive melt transport in shallow subcontinental mantle xenoliths (Tok Cenozoic volcanic field , SE Siberia). Earth Planet. Sci. Lett. 272, 65–77. http://dx.doi.org/10.1016/j.epsl.2008.04.020.
Toy, V.G., Prior, D.J., Norris, R.J., 2008. Quartz fabrics in the Alpine Fault mylonites: influence of pre-existing preferred orientations on fabric development during progressive uplift. J. Struct. Geol. 30 (5), 602–621. http://dx.doi.org/10.1016/j.jsg.2008.01.001.
Tullis, J., Yund, R.A., 1989. Hydrolytic weakening of quartz aggregates: the effects of water and pressure on recovery. Geophys. Res. Lett. 16 (11), 1343–1346.
Tullis, J., Christie, J.M., Griggs, D.T., 1973. Microstructures and preferred orientations of experimentally deformed quartzites. Geol. Soc. Am. Bull. 84 (January), 297–314.
Valcke, S.L.A., Casey, M., Lloyd, G.E., Kendall, J.-M., Fisher, Q.J., 2006. Lattice preferred orientation and seismic anisotropy in sedimentary rocks. Geophys. J. Int. 166 (2), 652–666. http://dx.doi.org/10.1111/j.1365-246X.2006.02987.x.
Vauchez, A., Garrido, C.J., 2001. Seismic properties of an asthenospherized lithospheric mantle: constraints from lattice preferred orientations in peridotite from the Ronda massif. Earth Planet. Sci. Lett. 192 (2), 235–249. http://dx.doi.org/10.1016/S0012-821X(01)00448-4.
Vauchez, A., Tommasi, A., Mainprice, D., 2012. Faults (shear zones) in the Earth's mantle. Tectonophysics 558-559, 1–27. http://dx.doi.org/10.1016/j.tecto.2012.06.006.
Vaughan, M.T., Weidner, D.J., 1978. The relationship of elasticity and crystal structure in andalusite and sillimanite. Phys. Chem. Miner. 3, 133–144.
Ward, D., Mahan, K., Schulte-Pelkum, V., 2012. Roles of quartz and mica in seismic anisotropy of mylonites. Geophys. J. Int. 190 (2), 1123–1134. http://dx.doi.org/10.1111/j.1365-246X.2012.05528.x.
Weidner, D.J., Wang, H., Ito, J., 1978. Elasticity of orthoenstatite. Phys. Earth Planet. Inter. 17, 7–13.

Weiss, T., Siegesmund, S., Rabbel, W., Bohlen, T., Pohl, M., 1999. Seismic velocities and anisotropy of the lower continental crust: a review. Pure Appl. Geophys. 156 (1–2), 97–122. http://dx.doi.org/10.1007/s000240050291.

Wenk, H.-R., Christie, J.M., 1991. Comments on the interpretation of deformation textures in rocks. J. Struct. Geol. 13 (10), 1091–1110. http://dx.doi.org/10.1016/0191-8141(91)90071-P.

Wenk, H.-R., Canova, G., Molinari, a., Kocks, U.F., 1989. Viscoplastic modeling of texture development in quartzite. J. Geophys. Res. 94 (B12), 17895. http://dx.doi.org/10.1029/JB094iB12p17895.

Whitney, D.L., Evans, B.W., 2010. Abbreviations for names of rock-forming minerals. Am. Mineral. 95 (1993), 185–187. http://dx.doi.org/10.2138/am.2010.3371.

Zhang, Y., Hobbs, B.E., Jessell, M.W., 1994. The effect of grain-boundary sliding on fabric development in polycrystalline aggregates. J. Struct. Geol. 16 (9), 1315–1325.

Zhou, Y., Zhou, P., Wu, S.M., Bin Shi, X., Zhang, J.J., 2002. Magnetic fabric study across the Ailao Shan–Red River shear zone. Tectonophysics 346 (3–4), 137–150. http://dx.doi.org/10.1016/S0040-1951(01)00269-4.